

MICROCOPY RESOLUTION TEST CHART
NATIONAL BUREAU OF STANDARDS-1963-A

REPORT NO. NADC-83053-60

(12)



A STUDY OF POLYMER MATRIX FATIGUE PROPERTIES

Edwin M. Odom and Donald F. Adams
Composite Materials Research Group
Mechanical Engineering Department
UNIVERSITY OF WYOMING
Laramie, Wyoming 82071

JUNE 1983

FINAL REPORT
Contract No. N62269-80-C-0278

APPROVED FOR PUBLIC RELEASE; DISTRIBUTION UNLIMITED

NOV 29 1983
A

Prepared for
Aircraft and Crew Systems Technology Directorate
NAVAL AIR DEVELOPMENT CENTER
Warminster, PA 18974

88 11 28 207

AD-A135 076

~~DTIC FILE COPY~~

NOTICES

REPORT NUMBERING SYSTEM – The numbering of technical project reports issued by the Naval Air Development Center is arranged for specific identification purposes. Each number consists of the Center acronym, the calendar year in which the number was assigned, the sequence number of the report within the specific calendar year, and the official 2-digit correspondence code of the Command Office or the Functional Directorate responsible for the report. For example: Report No. NADC-78015-20 indicates the fifteenth Center report for the year 1978, and prepared by the Systems Directorate. The numerical codes are as follows:

CODE	OFFICE OR DIRECTORATE
00	Commander, Naval Air Development Center
01	Technical Director, Naval Air Development Center
02	Comptroller
10	Directorate Command Projects
20	Systems Directorate
30	Sensors & Avionics Technology Directorate
40	Communication & Navigation Technology Directorate
50	Software Computer Directorate
60	Aircraft & Crew Systems Technology Directorate
70	Planning Assessment Resources
80	Engineering Support Group

PRODUCT ENDORSEMENT – The discussion or instructions concerning commercial products herein do not constitute an endorsement by the Government nor do they convey or imply the license or right to use such products.

REPORT DOCUMENTATION PAGE		READ INSTRUCTIONS BEFORE COMPLETING FORM
1. REPORT NUMBER NADC-83053-60	2. GOVT ACCESSION NO.	3. RECIPIENT'S CATALOG NUMBER
4. TITLE (and Subtitle) A Study of Polymer Matrix Fatigue Properties		5. TYPE OF REPORT & PERIOD COVERED September 1979-February 1983 Final Report
		6. PERFORMING ORG. REPORT NUMBER UWME-DR-301-103-1
7. AUTHOR(s) Edwin M. Odom Donald F. Adams		8. CONTRACT OR GRANT NUMBER(s) N62269-80-0278
9. PERFORMING ORGANIZATION NAME AND ADDRESS The University of Wyoming University Station, Box 3295 Laramie, WY 82071		10. PROGRAM ELEMENT, PROJECT, TASK AREA & WORK UNIT NUMBERS
11. CONTROLLING OFFICE NAME AND ADDRESS Aircraft Crew Systems Technology Directorate Naval Air Development Center Warminster, PA 18974		12. REPORT DATE June 1983
		13. NUMBER OF PAGES 120
14. MONITORING AGENCY NAME & ADDRESS (if different from Controlling Office)		15. SECURITY CLASS. (of this report) Unclassified
		15a. DECLASSIFICATION/DOWNGRADING SCHEDULE
16. DISTRIBUTION STATEMENT (of this Report) Approved for Public Release; Distribution Unlimited		
17. DISTRIBUTION STATEMENT (of the abstract entered in Block 20, if different from Report)		
18. SUPPLEMENTARY NOTES		
19. KEY WORDS (Continue on reverse side if necessary and identify by block number)		
Epoxy Shear Bismaleimide Temperature Effects Fatigue Specimen Fabrication Tension Scanning Electron Microscopy		
20. ABSTRACT (Continue on reverse side if necessary and identify by block number)		
<p>→ Hercules 3501-6 neat epoxy and Hercules X4001 neat bismaleimide specimens were fabricated and tested, both statically and in cyclic fatigue. Axial tensile and torsional shear loadings were utilized, at room temperature and 88°C.</p> <p>Detailed procedures are given for casting good quality specimens of these high performance structural polymers in neat (unreinforced) form. Techniques are also presented for gripping the specimens for mechanical loading, with special emphasis on problems which can be anticipated during fatigue cycling.</p>		

Unclassified

10000

CONFIDENTIAL
SECURITY CLASSIFICATION OF THIS PAGE(When Data Entered)

Although there was scatter in the fatigue data for these relatively brittle polymers, the S-N curves exhibited a knee at about 10^4 cycles. That is, an endurance limit is suggested, which it may be possible to correlate with corresponding composite material response.

Extensive scanning electron microscopy (SEM) was performed on the neat resin fracture surfaces. Failure initiation sites and a consistent pattern of crack propagation were exhibited. The observations suggest that the failures of the torsion specimens were consistently via tensile mode, characteristic of brittle materials. Correlations were made between the relative sizes of the fractures observed, and the static strengths and fatigue lives of the materials.

11
Unclassified

SECURITY CLASSIFICATION OF THIS PAGE(When Data Entered)

PREFACE

This Final Report summarizes a two-year research program initiated in September 1979, sponsored by the Naval Air Development Center. The NADC Program Monitor was Mr. Lee W. Gause.

All work was performed by the Composite Materials Research Group within the Mechanical Engineering Department at the University of Wyoming. Co-Principal Investigators were Mr. Edwin M. Odom, Staff Engineer and Dr. Donald F. Adams, Professor. Mr. David E. Walrath, Staff Engineer, also served as a Principal Investigator during the initial phases of the study. Others making significant contributions included Undergraduate Students Anthony Vercimak, David Cortes, Gregory Morrison, Matthew Graf and Patrick Bishop, and Graduate Students Norris Shippen, Raja Mohan and Jayant Mahishi. In particular, Mr. Mahishi performed the specimen failure analysis of Section 5.



Title	
Author	
Sponsor	
Classification	
Distribution/Availability Codes	
Dist	Avail and/or Special
AI	

TABLE OF CONTENTS

	<u>Page</u>
SECTION 1 INTRODUCTION AND SUMMARY	1
1.1 Introduction	1
1.2 Summary	2
SECTION 2 SPECIMEN CONFIGURATIONS AND TEST METHODS	3
2.1 Specimen Configurations	3
2.2 Specimen Gripping	8
2.3 Test Matrix	11
SECTION 3 EXPERIMENT RESULTS	15
3.1 Tensile and Shear Fatigue Results	15
3.2 Specimen Self-Heating	25
SECTION 4 SCANNING ELECTRON MICROSCOPY OBSERVATIONS	27
4.1 Specimen Preparation	27
4.2 Typical SEM Photographs of Specimen Failure Surfaces	28
4.3 Summary of SEM Observations	39
4.4 Interpretation of Specimen Failure Processes	40
SECTION 5 ANALYSIS OF SPECIMEN FAILURES CAUSED BY ENVIRONMENTAL CHAMBER MALFUNCTION	45
5.1 Description of Malfunction	45
5.2 Experimental Observations	45
5.3 Analysis Approach	47
5.4 Finite Element Analysis	51
5.4.1 Transient Axisymmetric Moisture Distribution Program (TAXIMD)	52
5.4.2 Stress Analysis of Crack Initiation Propagation	57
5.5 Discussion	57
SECTION 6 CONCLUSIONS AND SUGGESTIONS FOR FUTURE WORK	61
6.1 Conclusions	61
6.2 Suggestions for Future Work	61
REFERENCES	63
APPENDICES	67
APPENDIX A NEAT RESIN CASTING TECHNIQUES	69
APPENDIX B INDIVIDUAL TEST RESULTS	77
APPENDIX C ROTOMETER DESCRIPTION AND THEORY OF OPERATION	87
APPENDIX D SEM PHOTOGRAPHS OF SPECIMEN FAILURE SURFACES	91
APPENDIX E MOISTURE DISTRIBUTION ANALYSIS PARAMETERS	117

SECTION 1

INTRODUCTION AND SUMMARY

1.1 Introduction

The Composite Materials Research Group at the University of Wyoming has been performing research on the mechanical and physical behavior of neat epoxy resins for over seven years. This research was initiated to provide constituent properties for use in micromechanics analyses of composite materials concurrently developed by the Composite Materials Research Group. Previous results of this work are presented in References [1-6], among other publications.

One area of research related to the properties of neat resin that has not received much attention involves fatigue response. The objective of the present program therefore was to continue previous work for NADC [7], to supplement this information.

The present program entailed tension-tension and non-reversed torsion cyclic loading of a neat (unreinforced) epoxy system, Hercules 3501-6, and a neat bismaleimide system, Hercules X4001, at ambient and elevated temperatures. The Hercules 3501-6 epoxy is a 177°C (350°F) cure system while the Hercules X4001 bismaleimide is a 204°C (400°F) cure system [8]. To perform this testing, high quality neat resin specimens first had to be fabricated. Two different techniques were developed during this program to successfully fabricate these specimens. Full details of these methods are presented in Appendix A.

Static tensile tests were conducted at a rate of 2mm/min, while torsion tests were conducted at 1 rad/min. All static testing was performed in an Instron Model 1125 electromechanical testing machine.

The tensile fatigue testing was performed in an MTS Model 810 servohydraulic testing machine at 10 cycles/second, while the torsional fatigue testing was performed in an Instron Model 1321 servohydraulic testing machine at 3 cycles/sec. All fatigue tests were conducted using an R ratio (minimum stress divided by peak stress) of 0.1.

Failed specimens from the static and fatigue tests were subsequently examined utilizing a Scanning Electron Microscope (SEM) to identify the failure modes.

1.2 Summary

It was found that both neat resin matrix materials, at both test temperatures, and for both tensile and torsion fatigue, exhibited a reduction in strength versus number of cycles initially. However, at a defined number of fatigue cycles, a threshold seemed to occur such that there was little or no further reduction in fatigue strength with increasing number of cycles, i.e., a knee in the S-N curve exists. The exact location of this knee in terms of stress level and number of cycles was difficult to define.

Establishing the correct way of gripping neat resin fatigue specimens to prevent failure in the gripped area of the specimen was difficult. However after many trials, several general rules to minimize this problem were developed, which will be discussed in Section 2.

During the course of the present program, a moisture-preconditioning chamber failure occurred, the rapid loss of humidity causing most of the specimens in the chamber at the time to crack due to stresses induced by the high moisture gradient which developed. A study was performed to better understand this phenomenon, the results being presented in Section 5.

SECTION 2

SPECIMEN CONFIGURATIONS AND TEST METHODS

2.1 Specimen Configurations

In order to generate valid mechanical properties test data, it is first necessary to develop a proper specimen geometry. It must then be practical to fabricate specimens to the geometry developed. Perhaps the most important design aspect to note is that neat resins do not have the same general behavior as metals. Therefore, utilizing a specimen geometry which was developed for, and is well-suited to, metals will not necessarily be successful. Since other groups may be interested in testing neat resin specimens in the future, this section will include general guidelines on the proper specimen geometries needed to test neat resins. These guidelines will primarily deal with developing specimen geometries for cyclic loading. It was found during this study that a neat resin specimen geometry that can be successfully fatigue tested can also be utilized for static testing. That is, testing in cyclic fatigue is the more difficult task.

During the present program, two specimen geometries were utilized, viz, a flat, rectangular cross section, dogbone-shaped specimen for tensile tests, and a round cross section dogboned specimen for torsion tests. These specimen geometries are shown in Figure 1. As stated previously, there are general guidelines to be followed in establishing a proper specimen geometry. In general the specimen must be dogboned, to reduce the cross-sectional area in the central region of the specimen and thereby force failure into the center portion of the specimen away from the gripping region.



Figure 1. Geometry of Specimens for Static and Cyclic Tests (Top - Tensile Specimens, Bottom - Torsion Specimens).

This is a standard consideration when testing materials. Special difficulties arise when testing neat resin, however, due to the typically brittle nature of these materials. In fact, the difficulty arises not in the gage length, but in the gripped area of the specimen.

It was found that any stress concentration caused by gripping forces, or unevenness of the gripping faces, could be severe enough to cause specimen failure in the gripped section of the specimen during cyclic loading. By successive trials it was found that the optimum applied shear stress on the gripped section of the specimen should be about 700 kPa (100 psi). This value was then utilized to design the flat tensile specimens. The method utilized to calculate this value is shown in Figure 2. Unfortunately, this value was established only after experiencing severe gripping difficulties with the round torsion specimen, which was designed with a larger value of the applied gripping

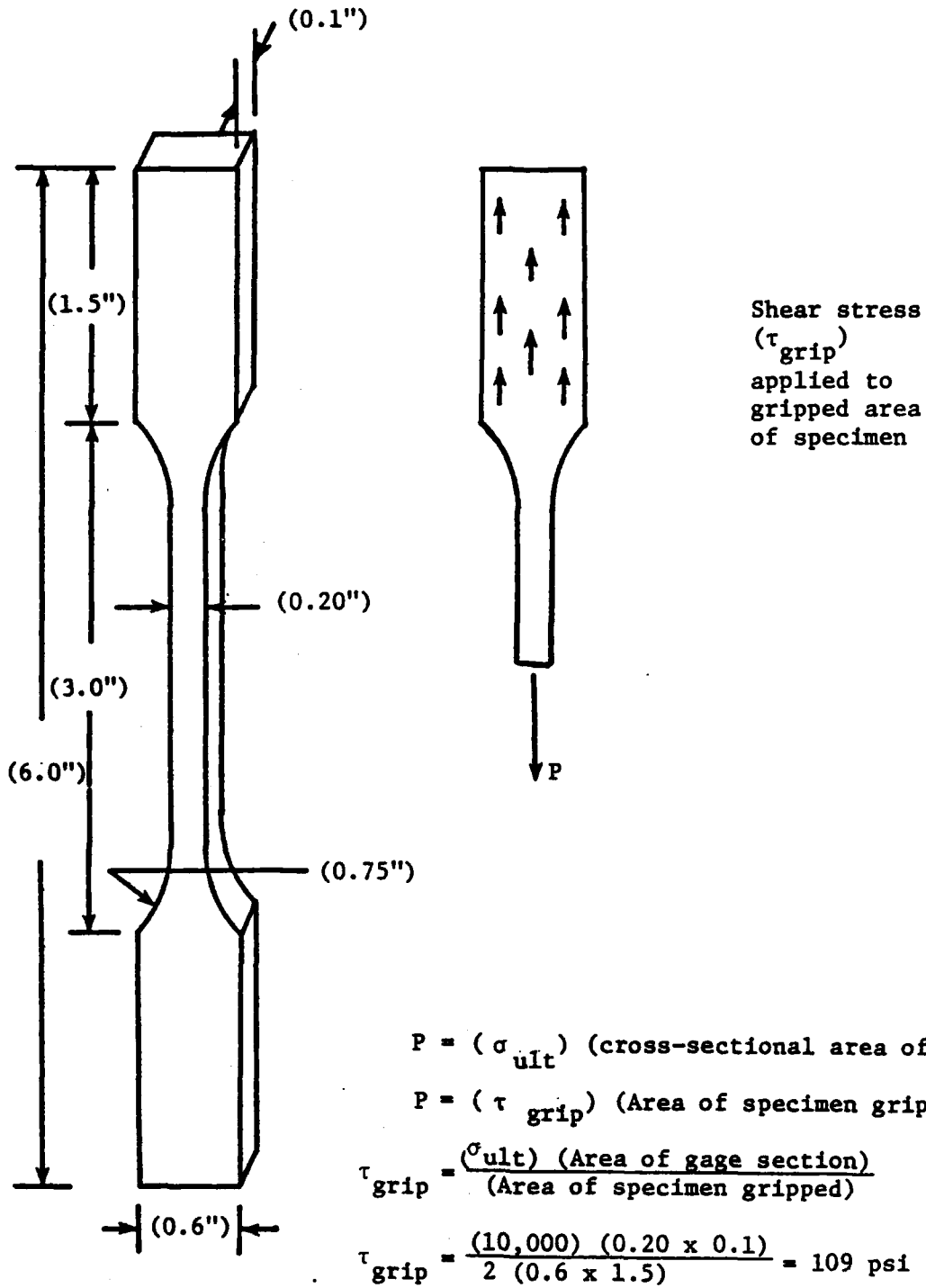
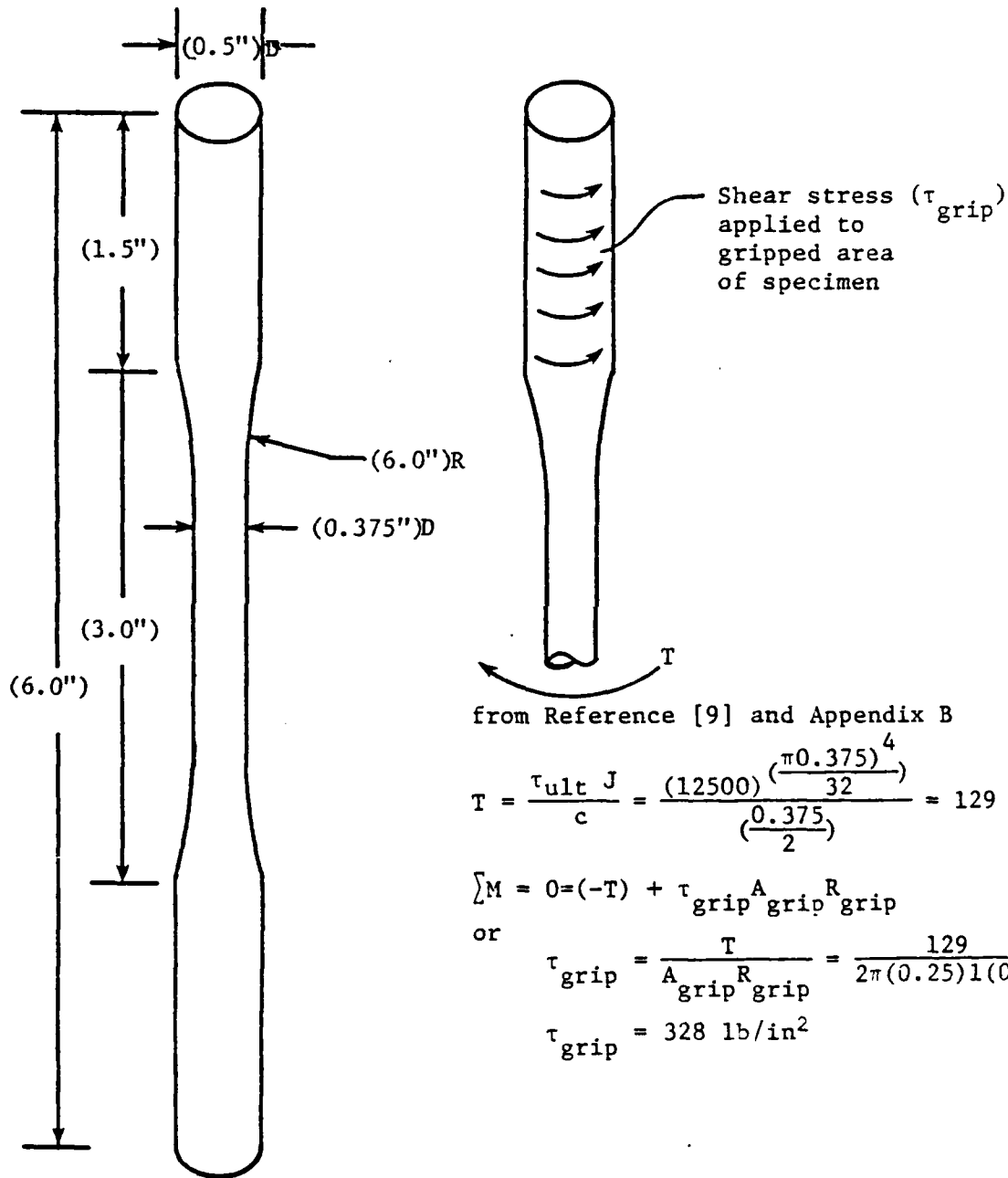


Figure 2. Method Utilized to Calculate Maximum Gripping Shear Stress Needed for Tensile Specimens

shear stress. The gripping shear stress value utilized for the round specimen was about 2.2 MPa (325 psi). The method utilized to calculate this value is shown in Figure 3.

It should be noted that a comparison of the calculated gripping shear stress value to the ultimate shear strengths of the materials tested and reported in Appendix B indicates the gripping shear stress values are only about one to three percent of the ultimate shear strengths. This would seem to be unnecessarily low. However, there are two equally important factors involved in obtaining the gripping shear stress i.e., the coefficient of friction between the grip faces and the specimen, and the gripping force. If the coefficient of friction is low, the gripping force must therefore be high. This creates a problem in that a stress concentration occurs in the specimen in the region of the specimen where the grip face first comes into contact. If the coefficient of friction is increased, the gripping force can be reduced. The difficulty here is that to get a higher coefficient of friction between the specimen and the grip face requires that the grip face be rough. However, the roughened faces can and will cause a stress concentration in the specimen, leading to premature failure. The margin between success and failure in gripping neat resin specimens during cyclic loading tests can be quite small. For instance, it was found that bonding 400-grit emery paper to the grip faces would allow the specimen to be successfully fatigue tested without specimen slippage or failure in the grips. However, using 150-grit emery paper consistently caused failure in the grip region.

An important aspect in eventually solving the gripping problem in this study was that the Hercules 3501-6 neat resin is optically



from Reference [9] and Appendix B

$$T = \frac{\tau_{ult} J}{c} = \frac{(12500) \left(\frac{\pi(0.375)^4}{32} \right)}{\left(\frac{0.375}{2} \right)} = 129 \text{ in-lb}$$

$$\sum M = 0 = (-T) + \tau_{grip} A_{grip} R_{grip}$$

or

$$\tau_{grip} = \frac{T}{A_{grip} R_{grip}} = \frac{129}{2\pi(0.25)1(0.25)}$$

$$\tau_{grip} = 328 \text{ lb/in}^2$$

Figure 3. Method Utilized to Calculate Maximum Gripping Shear Stress Needed for Torsion Specimens.

transparent and also photoelastic (birefringent). A considerable effort was expended in observing specimens under load with a polariscope, to evaluate the gripping problems encountered. This information is presented here in order to provide future investigators a tool to solve new gripping problems should they occur.

One further aspect of torsion specimen design, which is not often considered, is the total specimen rotation to be required. This dictates the required grip and actuator rotation capability of the testing machine. For the specimens of the present study, the length of the specimen subjected to torsion was 7.6 cm (3 in), the diameter of the gage section was 0.95 cm (0.375 in), and the ultimate shear strength was assumed to be 86 MPa (12.5 ksi), the highest value measured for the resin systems of this study (see Appendix B), the shear modulus being 1.76 GPa (0.25 Msi). From Reference [9]:

$$T = \frac{\tau J}{c} \quad \text{and} \quad \theta = \frac{TL}{JG}$$

where T = applied torque

τ = shear stress

J = polar moment of inertia

c = specimen radius

L = length of gage section

G = shear modulus

θ = rotation of specimen

Utilizing these two equations and the material properties and torsion specimen geometry presented yields a rotation of 46°. This is a very large actuator rotation. In fact, the highest frequency at which the Instron Model 1321 servohydraulic testing machine utilized in this study could operate was 4.5 Hertz for a 46° rotation. This frequency was

reduced to 3 Hertz for this study, primarily to insure that the actuator could follow the command signal precisely, and secondarily to prevent excessive wear on the testing machine hydraulic hoses, which tended to excessively vibrate at frequencies over 3 Hertz. The important point to be obtained from the above example is that test machine performance must be considered in the specimen design phase if the testing frequency is fixed.

2.2 Specimen Gripping

Two different grips were utilized for testing the neat resin specimens. For the flat-sided specimens, Instron Model 2710-003, 1000-pound capacity, Screw-Action Grips were utilized. These grips are indicated in Figure 4. One face of these grips is adjustable to compensate for specimen thickness, thus allowing for specimen alignment. The other face clamps against the specimen. An important feature of these grips is a nylon compression washer which prevents the clamping pressure from decaying during cyclic loading. These grips worked very well in terms of not slipping, and also in minimizing specimen breakage at the grip.

It should be noted that standard wedge grips were initially tried for tensile fatigue cycling of neat resin specimens. Typically, the specimen failed in the grips. This was attributed to the wedge action of these grips continually increasing the gripping pressure during cyclic loading. Wedge-action grips did work well for static testing, however.

Torsion fatigue specimens were gripped utilizing collets. This grip is indicated in Figure 5. These grips were designed and fabricated in-house, for specific use in this program. For applied shear stress



Figure 4. Instron Screw-Action Grip Utilized for Tension Fatigue Specimen

levels up to about 41 MPa (6 ksi) for the specimen geometry utilized in this program, these grips worked well. Above this stress level, either the grips tended to slip, or the gripping pressure was high enough to induce failure in the gripped area of the specimen. As a result of these gripping problems, specimens could not be cycled with confidence at stresses higher than about 41 MPa.

Reasons for these grips not performing as well as expected at high stress levels will be presented here, in the spirit of providing future investigators general information on the gripping of neat resin specimens. The major difficulty in gripping round specimens is associated with the geometry. To successfully grip a neat resin

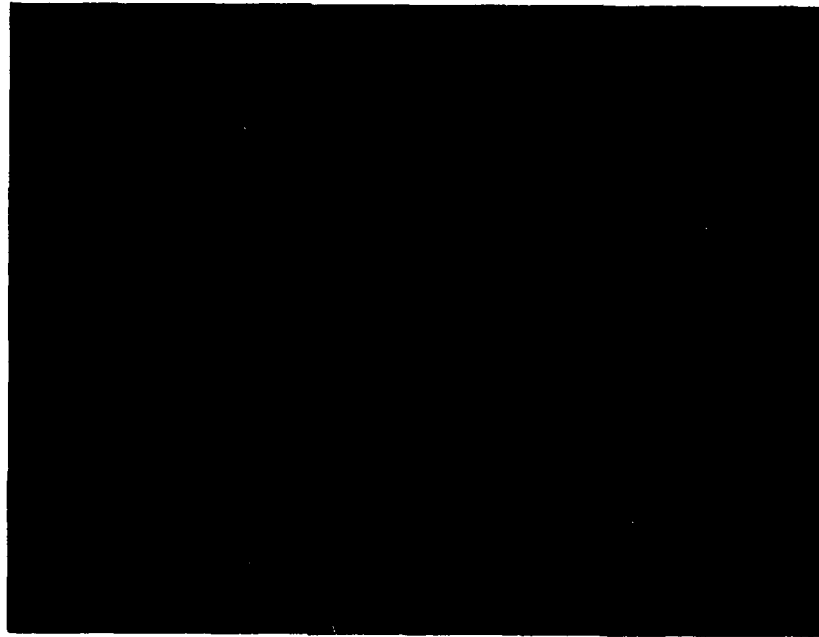


Figure 5. Collet Grip Utilized for Torsion Fatigue Specimens

specimen, a low clamping pressure over a large area is needed. In gripping a round specimen, a difficulty arises in that for the round specimen to be inserted into a collet grip, the radius of curvature of the grip area has to be larger than the radius of curvature of the specimen. However, during the clamping of the specimen, the radius of curvature of the collet grip does not change. The specimen thus tends to come into line contact with each of the centers of the the tangs of the collet when it is tightened. Therefore, the area available to apply the clamping force is limited. The approach utilized in the present study to eliminate this problem entailed lining the inside of the collet with 400-grit emery paper to increase the gripping action and to distribute the clamping pressure more uniformly. This allowed the cyclic loading of the specimens utilized in this study up to an applied

stress of about 41 MPa (6 ksi), as previously noted. The second problem in gripping round specimens with the collet grips utilized is that a mechanism for preventing clamping pressure decay with time (relaxation) is not available. Many of the specimens tested at higher stress levels required intermittent tightening of the collet grips during the fatigue test, to prevent specimen slippage. Future work on torsion fatigue testing of neat resin specimens should include additional attention to grip design and verification.

2.3 Test Matrix

The original test matrix for this program included tension-tension, tension-compression, compression-compression and nonreversed torsion cyclic loading. Additionally, each of these loading modes was to be performed at room temperature with no moisture conditioning, and at 66°C (150°F) with specimens fully moisture-saturated. However, due to the gripping difficulties explained previously, the test matrix had to be modified.

Specimen gripping problems suggested the elimination of tension-compression and compression-compression loading modes. The problem encountered was that compression specimens require a large cross-sectional area in the gage section to prevent buckling. This necessitates very high gripping shear stresses, to induce high loadings in the specimen. As explained earlier, high gripping shear stresses are not acceptable when conducting fatigue tests.

Moisture-saturated specimens were eliminated due to fully moisture-saturated specimens having a tendency to crack due to moisture-induced stresses. This problem actually was observed three times. The first and third times were after a minor humidity chamber

malfunction occurred, causing the chamber to lose humidity. The specimens started to rapidly dry out at their surfaces, causing a steep moisture gradient that induced very high hoop stresses in the round dog-boned specimens, leading to failure by surface cracking. The second observation of moisture-induced specimen failure occurred when cyclic loading testing was attempted. Since a test chamber which could control both temperature and relative humidity was not available, the moisture-preconditioned specimens were wrapped with a damp cloth to prevent specimen dryout during testing. Periodically this cloth was dampened. This approach was successful in protecting the gage section. However, the portion of the specimen engaged by the grips could not be kept damp and consequently moisture-induced cracking occurred there. Since this problem of specimen dryout could be encountered by future investigators as well, it was modeled analytically to identify the mechanisms that cause specimen failure. The results of this study are presented in Section 5.

As a result of the problems identified, the original test matrix was modified. The test matrix actually utilized in this study is presented in Table 1. All fatigue testing was performed with an R ratio of 0.1. For the static tensile tests, standard extensometers were utilized to measure axial strain. Since a device for measuring torsional strain was not available, a rotometer was developed in-house. Details of this device are included in Appendix C.

Table 1

Test Matrix for Fatigue Characterization of
Hercules 3501-6 and X4001 Resins

Material	Loading Mode	Test Environment	Static Tests	Fatigue Tests
3501-6	Tension- Tension (10 Hz)	RT, Dry	5	20
	Nonreversed Torsion (3 Hz)	RT, Dry	5	20
	Tension- Tension (10 Hz)	88°C, Dry	5	20
	Nonreversed Torsion (3 Hz)	88°C, Dry	5	20
X4001	Tension- Tension (10 Hz)	RT, Dry	5	20
	Nonreversed Torsion (3 Hz)	RT, Dry	5	20
	Tension- Tension (10 Hz)	88°C, Dry	5	20
	Nonreversed Torsion (3 Hz)	88°C, Dry	5	20
Totals			40	160

SECTION 3

EXPERIMENTAL RESULTS

3.1 Tensile and Shear Fatigue Results

The log cycles to failure versus peak tensile and shear stress plots for the Hercules 3501-6 and X4001 neat resins at room temperature and 88°C (190°F) are presented in Figures 6 through 13. Several general comments apply to all of these figures. First, there is evidence of a knee in every plot, and second, there is considerable variation in the cycles to failure for given stress levels. On each plot there are two lines drawn. The horizontal line is drawn at a constant stress level, the stress level at which it is estimated that the fatigue life would be 10^6 cycles or more. This line is extended to the left to 10^4 cycles. The second line is drawn from the stress level at 10^6 cycles (the static test value) to the intersection of the first line drawn and 10^4 cycles. Taken together, these two lines tend to represent the fatigue life (the S-N curve) of the material. However, it must be emphasized that the knee at 10^4 cycles is a defined value, based upon judgment. Therefore, these lines should only be interpreted as trend indicators.

In some instances the figures could be interpreted such that a straight line would fit the data of Figures 6 through 13. However, the method utilized for generating these plots must be considered when an interpretation is made. There are two general approaches for generating a S-N curve. The first method entails testing a set number of specimens at given stress levels. For example this approach might entail testing 5 specimens at 10 percent increments of the material ultimate strength. This method is recommended when very little knowledge of the fatigue

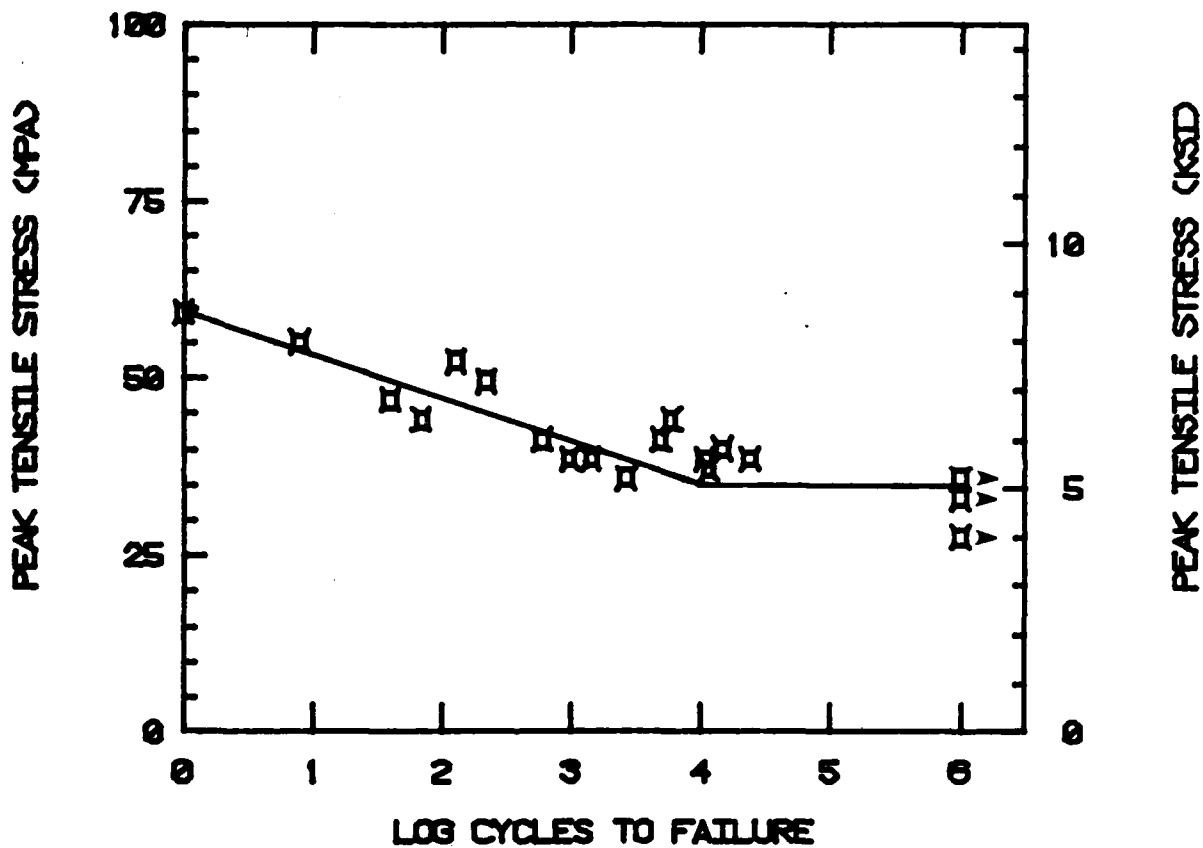


Figure 6. Tension-Tension Fatigue ($R = 0.1$) of Hercules 3501-6 Epoxy; Room Temperature, Dry.

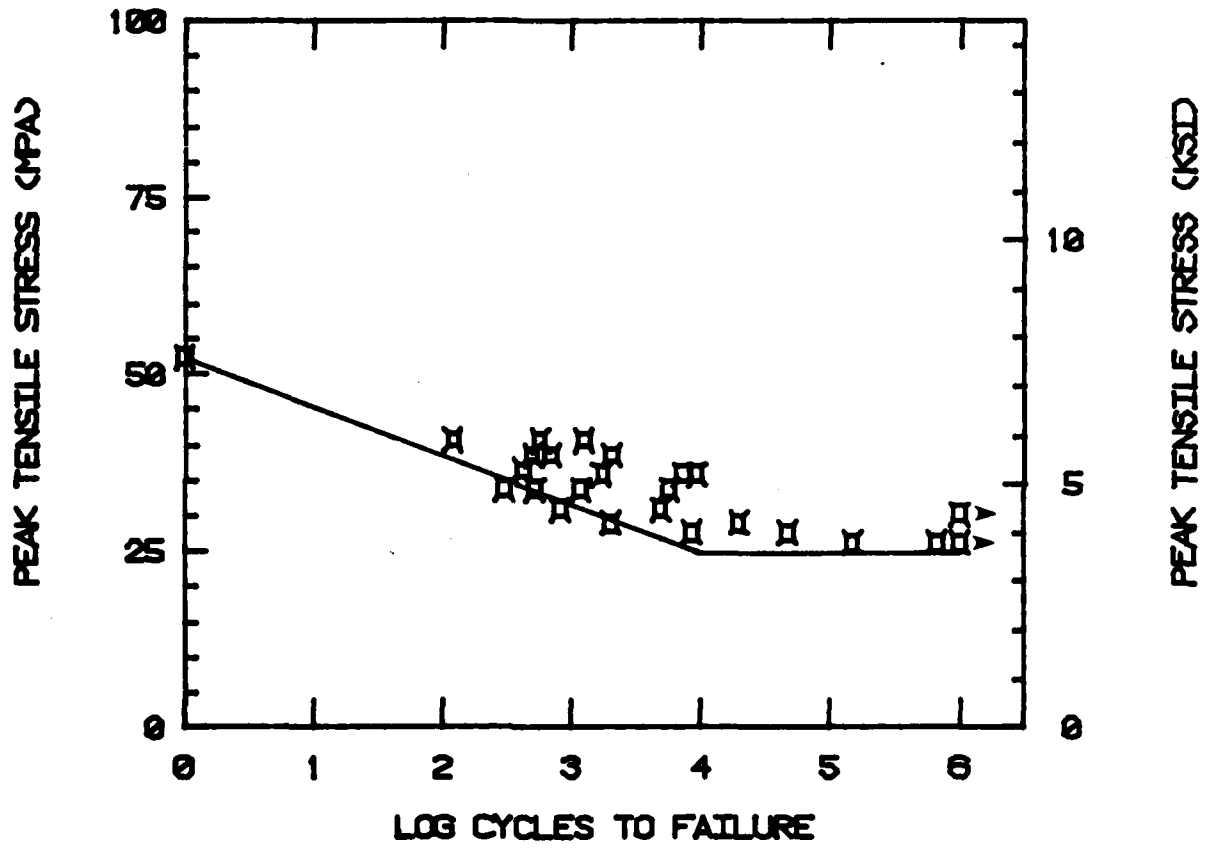


Figure 7. Tension-Tension Fatigue (R = 0.1) of Hercules 3501-6 Epoxy; 88°C (190° F), Dry.

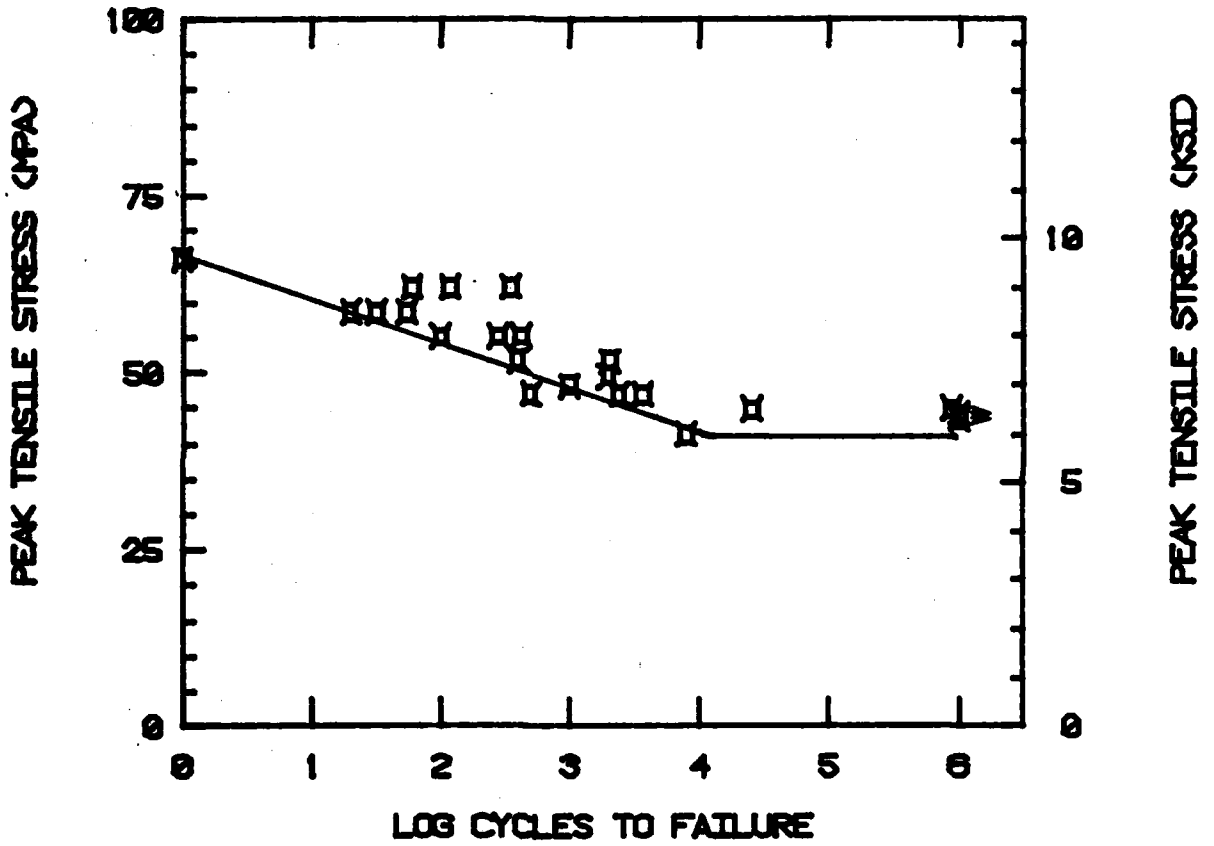


Figure 8. Tension-Tension Fatigue (R = 0.1) of Hercules X4001 Bismaleimide; Room Temperature, Dry.

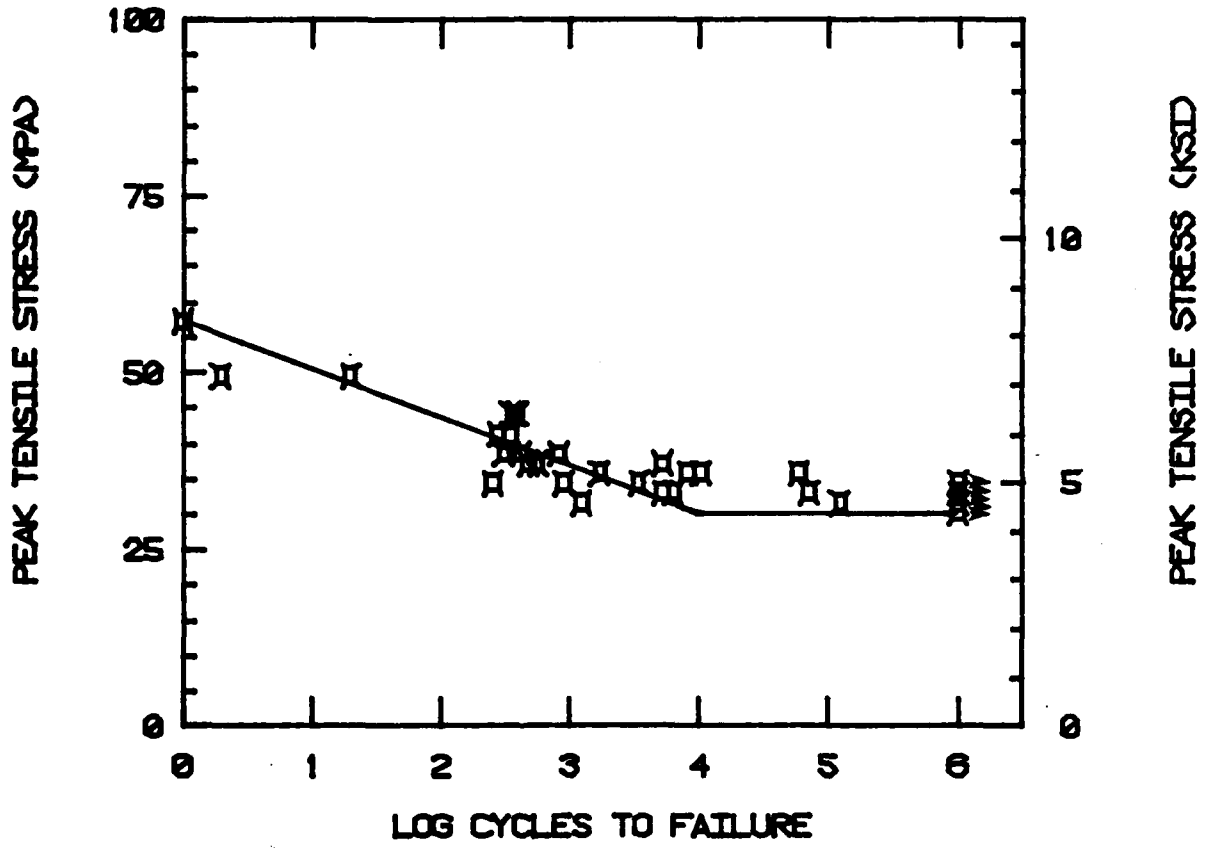


Figure 9. Tension-Tension Fatigue (R = 0.1) of Hercules X4001 Bismaleimide; 88°C (190°F), Dry.

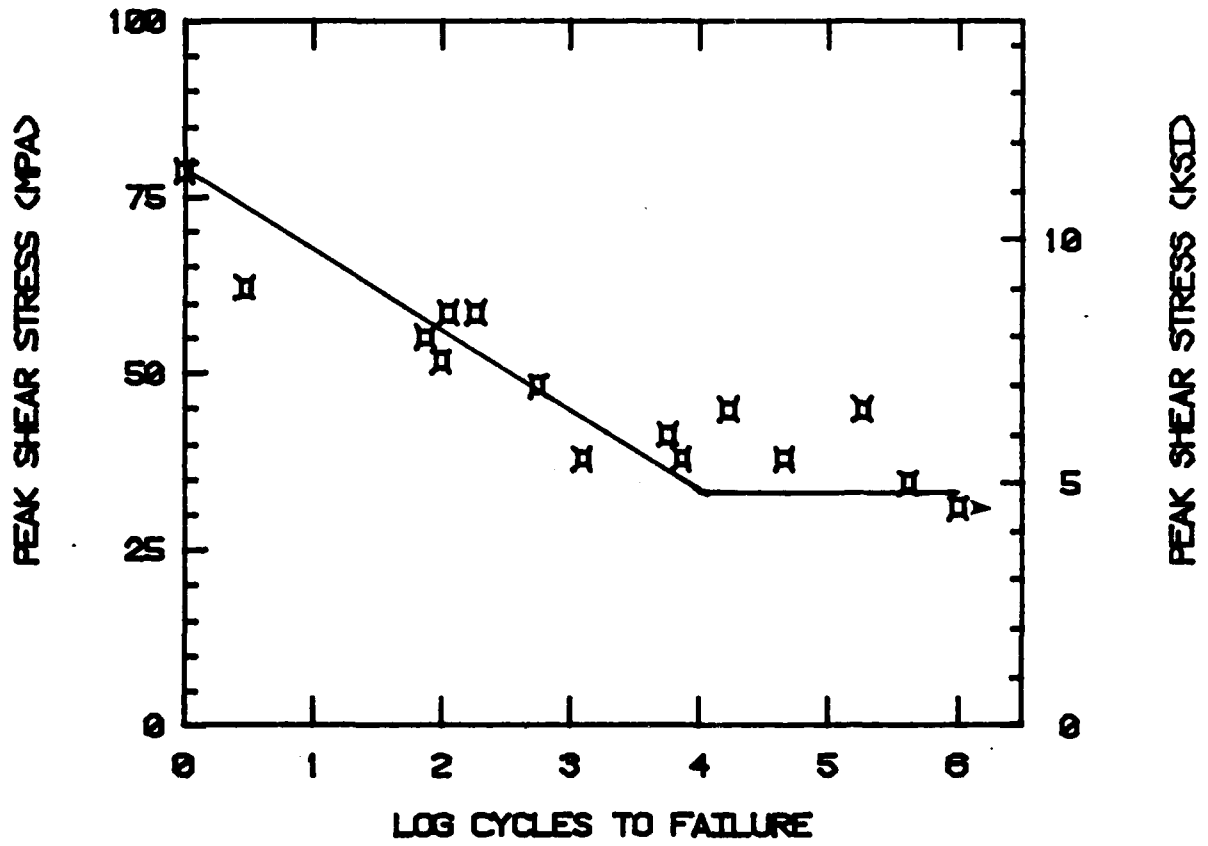


Figure 10. Torsional Fatigue (R = 0.1) of Hercules 3501-6 Epoxy; Room Temperature, Dry.

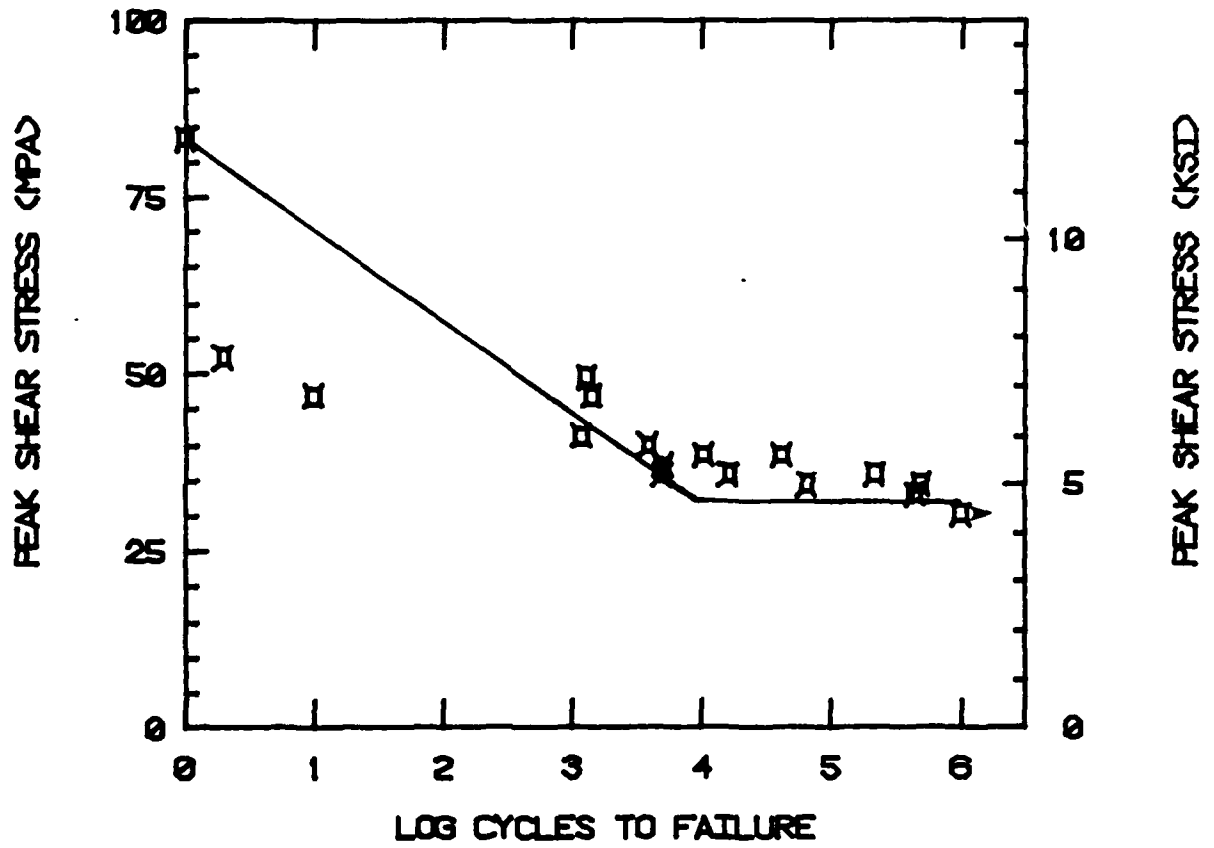


Figure 11. Torsional Fatigue ($R = 0.1$) of Hercules 3501-6 Epoxy; 88°C (190°F), Dry.

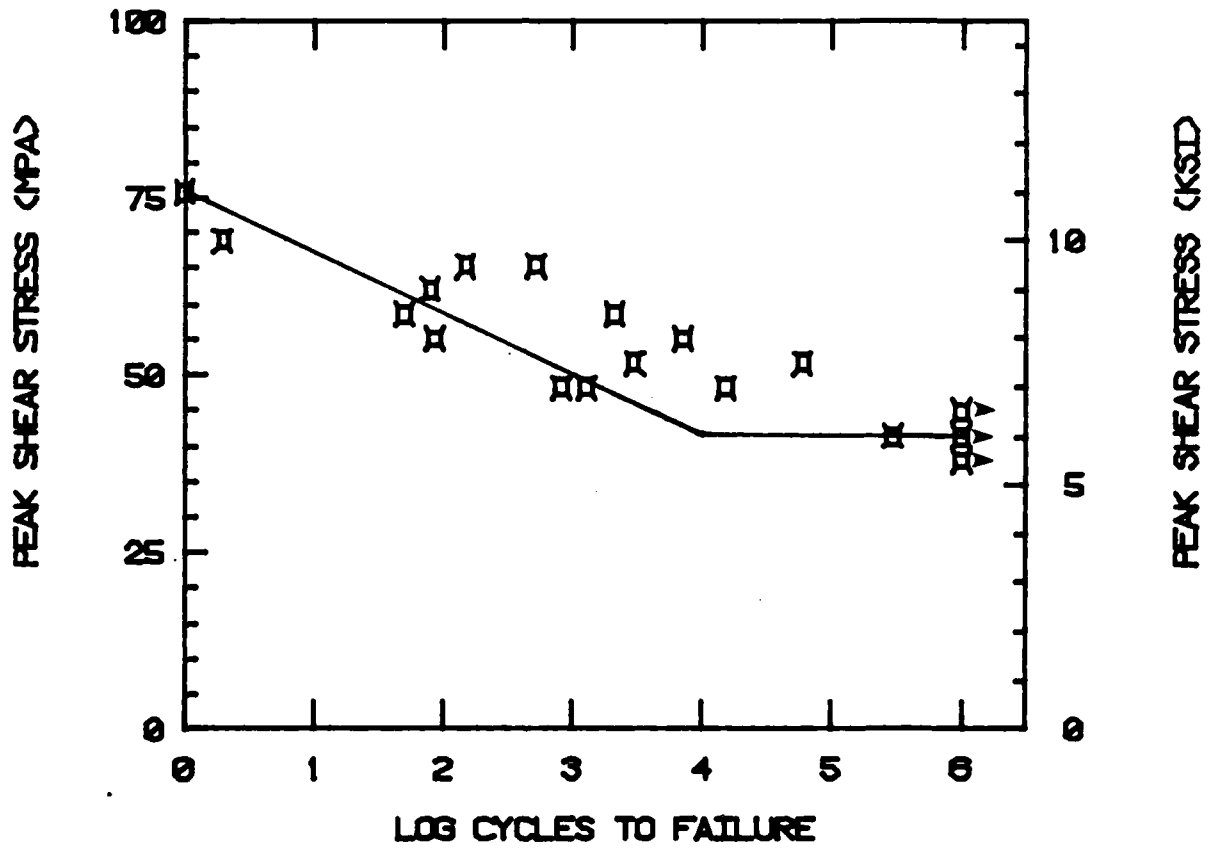


Figure 12. Torsional Fatigue (R = 0.1) of Hercules X4001 Bismaleimide; Room Temperature, Dry.

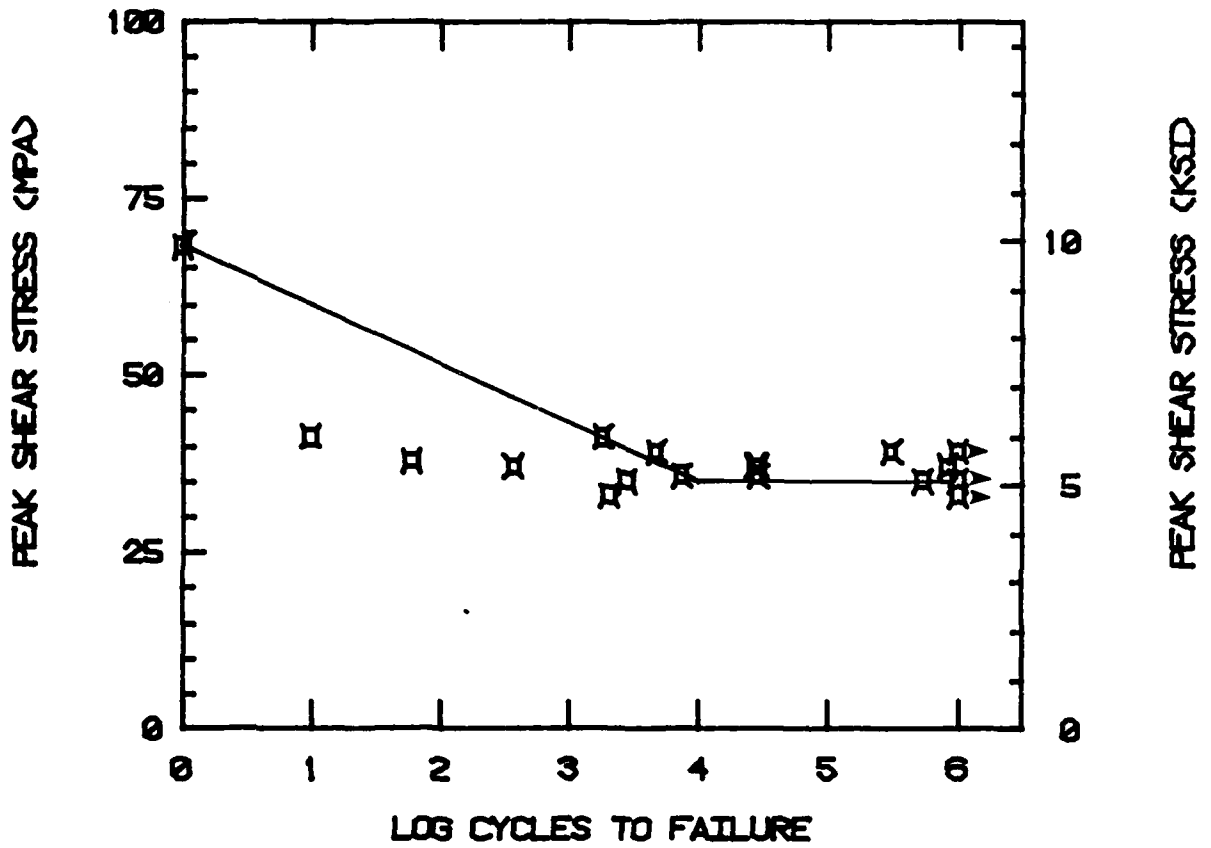


Figure 13. Torsional Fatigue (R = 0.1) of Hercules X4001 Bismaleimide; 88°C (190°F), Dry.

life is known about a particular material. The second approach entails testing several specimens at intermediate stress levels, for example, 75 percent of the ultimate material strength. A straight line drawn between these results and the static ultimate strengths is utilized as a guide to selecting the stress level of the next tests. As more specimens are tested this line is refitted to the test data. This approach works very well when the S-N curve is well behaved, i.e., linear when plotted on a semi-log scale. From previous work [7] it was believed that neat resins were well behaved and consequently this approach was utilized.

In generating the S-N curves utilizing the approach outlined above, it was found that at certain stress levels the specimens' fatigue life would begin to vary widely. Many of the S-N plots shown in Figures 6 through 13 indicate specimen fatigue lives that vary from less than 10^3 cycles to greater than 10^6 cycles at the same cyclic stress level. This type of material response is not well understood. It could suggest an endurance limit but the data is limited. Further, to prove the existence of an endurance limit would require very long tests, i.e., if the variation in fatigue life observed in this program continued, specimen cycles at lower peak stress levels would exhibit fatigue lives varying from 10^4 to 10^7 cycles or 10^5 to 10^8 cycles and so on. Tests of this duration are quite unreasonable to conduct from a time standpoint. Therefore, during the testing phase of this program when specimens began to have fatigue lives of 10^6 cycles at a certain stress level, additional tests were conducted at varying stress levels to try to define this apparent change in material behavior.

As stated previously, there is considerable variation in the cycles

to failure for given stress levels in the data plotted in Figures 6 through 13. Typically, when this variation in the data is anticipated, more test specimens are prepared and tested in an attempt to get a statistical average representing the true material behavior. The variation obtained during the present testing was not anticipated and therefore only limited additional specimens had been prepared. Available extra tensile test specimens of Hercules 3501-6 and X4001 were tested at 88°C (190°F), in an effort to further define the material fatigue response and the knee that was apparent in the S-N curves. Figures 7 and 9 indicate the S-N curves which include these additional data. In comparing these figures to the other S-N curves, additional specimens do improve the aesthetics of the S-N curve. However, the visual best-fit lines drawn on these plots in the same manner as the other plots do not fit any better or worse than on the other plots. It is concluded that it is desirable to utilize additional specimens when conducting fatigue tests on neat resins, but that a lesser number of specimens can give a very good understanding of the material behavior. It is suggested that future work be conducted utilizing 40 to 50 specimens for each S-N curve, rather than the 20 specimens utilized in the present program.

3.2 Specimen Self-Heating

Whenever polymer materials are subjected to cyclic loading, it is necessary to be concerned with specimen heating. This concern was addressed during the present study. Thermocouples were attached to specimens and the temperature was monitored at various stress levels. The largest temperature rise above ambient conditions recorded was 7°C (12°F), which occurred at room temperature for a Hercules 3501-6 tensile

specimen tested at approximately 65 percent of the static ultimate. Typically the temperature rise was 5 to 6°C (9 to 11°F) for both the Hercules 3501-6 and the Hercules X4001, and appeared to be independent of whether the test was tensile or torsion fatigue. Additionally, the temperature rise was not any greater for higher stress level tests, although this can somewhat be explained by the brevity of the test conducted at high stress levels.

After measuring the temperature rise and studying the fracture surfaces of the failed specimens (discussed in Section 4), several conclusions concerning specimen heating can be drawn. First, the S-N plots indicated in Figures 6 through 13 are not dependent on specimen heating. Second, test results of specimens tested at higher stress levels indicate the same failure mode (as will be presented in Section 4) as specimens tested at lower stress levels. This infers that overall specimen heating was not a factor in the failure process. Additionally, the temperature monitoring tests described previously verify that little specimen heating was evident.

SECTION 4

SCANNING ELECTRON MICROSCOPY OBSERVATIONS

4.1 Specimen Preparation

The Composite Materials Research Group has been utilizing the scanning electron microscope (SEM) in composite materials studies for over 10 years. However, very little has been done prior to the past two years in examining neat resin failures. At present very little is known about the causes of failure. After studying many SEM photographs, some insights into specimen failure modes can now be put forward. These insights are somewhat speculative, and are presented in the spirit of offering an initial explanation that the reader can accept, reject or modify based upon the reader's own experience.

Specimens were prepared for scanning electron microscope (SEM) observation by cutting the failure surface from the failed mechanical test specimens utilizing a Buehler No. 10-4150 silicon carbide cutoff disk. These failure surface specimens were bonded to one-inch diameter specimen mounts utilizing Ducco cement subsequently coated with conducting paint. The mounted specimens were ultrasonically cleaned to remove loose surface debris, and then vapor-coated with gold to make them electrically conductive. A conductive surface is necessary on nonconducting materials such as epoxy to minimize the accumulation of stray electrons on the fracture surface during SEM examination. This accumulation causes flaring during exposure to the electron beam. In the photograph to be presented here, there will occasionally be small areas where flaring did occur. These areas are typically very sharp or jagged surfaces of the specimen where the gold did not deposit.

When photographs of failure surfaces are taken with the SEM, an information banner is automatically placed across the bottom of the photograph. In the present photographs, this banner consists of gray alpha-numeric characters on a black background. Using Figure 14 of the next section as an example of what these characters mean:

25 kV	electron beam accelerating voltage, in kilovolts
X 22	magnification
4094	photograph number
100.0	length of scale, in micrometers (the letter u replaces the Greek symbol μ , representing micro)
UW 83	The SEM identification number, i.e., University of Wyoming and the current year 1983.

A total of 32 specimens were prepared for SEM observation. Of these specimens, eight had been subjected to static tensile testing and the remainder to fatigue testing. Photographs of the SEM observations will be presented in this section and in Appendix D. These photographs are presented in the spirit of providing a preliminary data base since relatively little SEM study of fracture surfaces of these structural epoxy resin materials has been performed in the past.

4.2 Typical SEM Photographs of Specimen Failure Surfaces

This section contains a sample of the many SEM photographs taken (see Figure 14 through 23), to illustrate the conclusions to be presented in the next section. Additional photographs are presented in Appendix C. For each specimen failure surface studied, up to four SEM photographs were taken, to fully document the fracture. All of these photographs will not be presented in this section; additional photographs are included in Appendix C.



a) Overall View of Specimen Failure Surface



b) Close-up of Failure Initiation Site

Figure 14. Static Tension, Specimen No. ZATL02, Room Temperature Test of Hercules 3501-6 Neat Epoxy Resin (Specimen Failed at 70.3 MPa, i.e., 10.2 ksi).

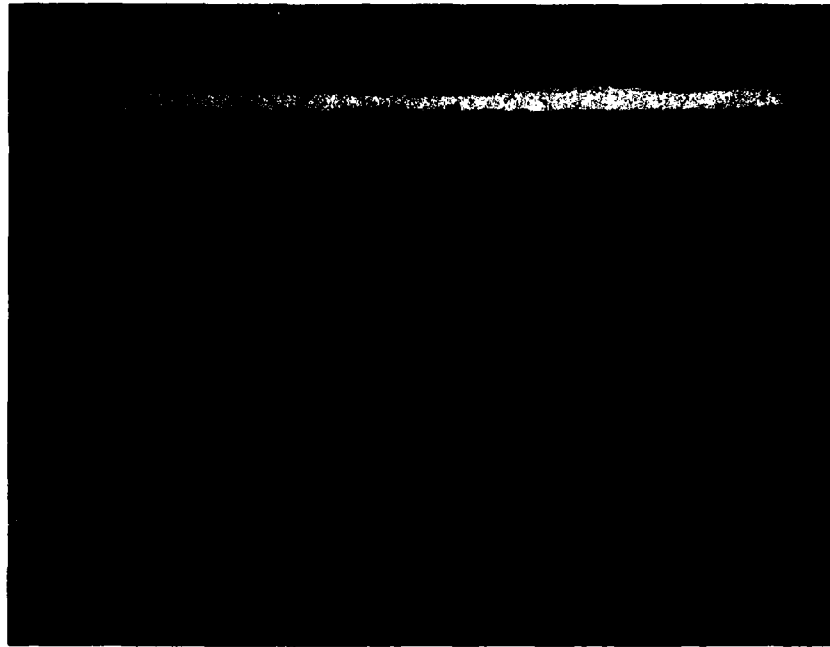


a) Overall View of Specimen Failure Surface



b) Close-up of Failure Initiation Site

Figure 15. Static Tension, Specimen No. ZATL03, Room Temperature Test of Hercules 3501-6 Neat Epoxy Resin (Specimen Failed at 68.2 MPa, i.e., 9.9 ksi).

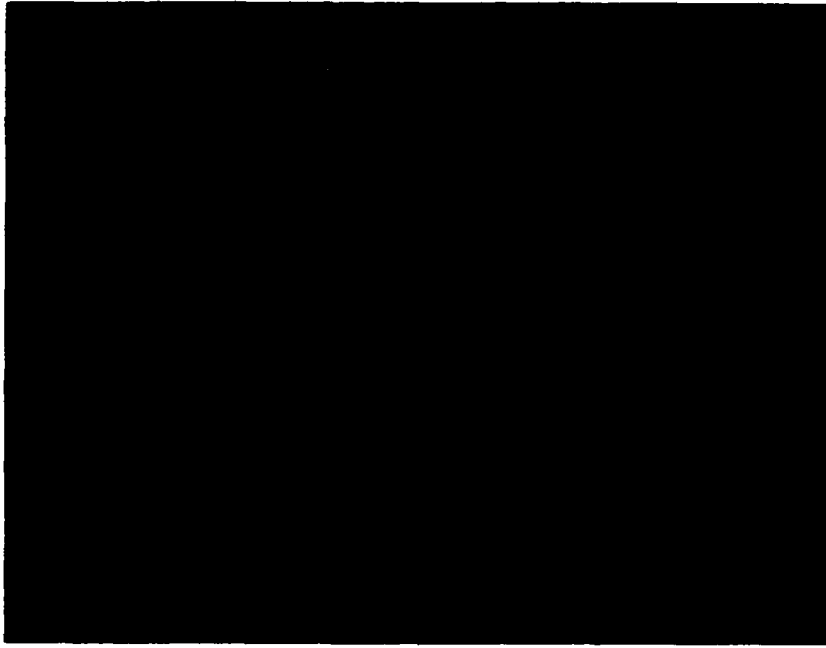


a) Overall View of Specimen Failure Surface

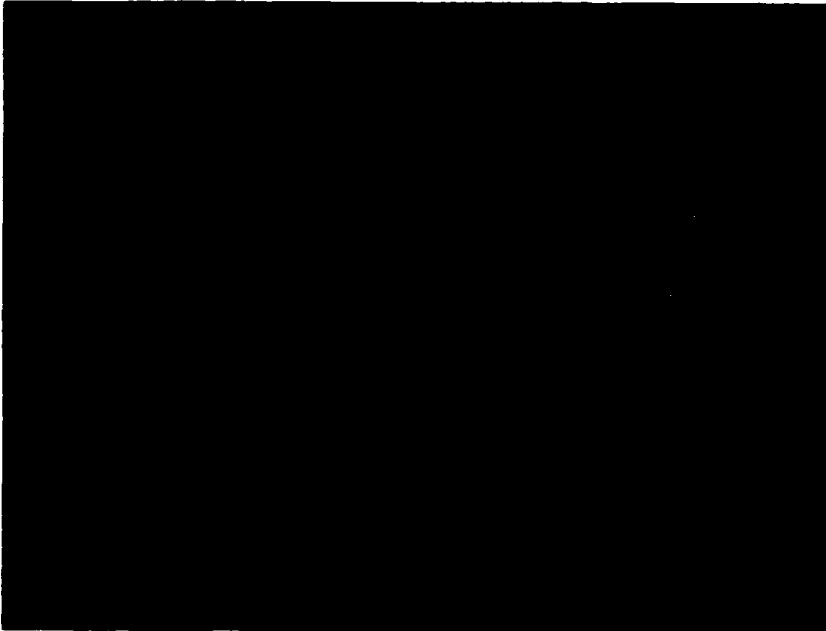


b) Close-up of Failure Initiation Site

Figure 16. Static Tension, Specimen No. ZATL04, Room Temperature Test of Hercules 3501-6 Neat Epoxy Resin (Specimen Failed at 50.3 MPa, i.e., 7.3 ksi).

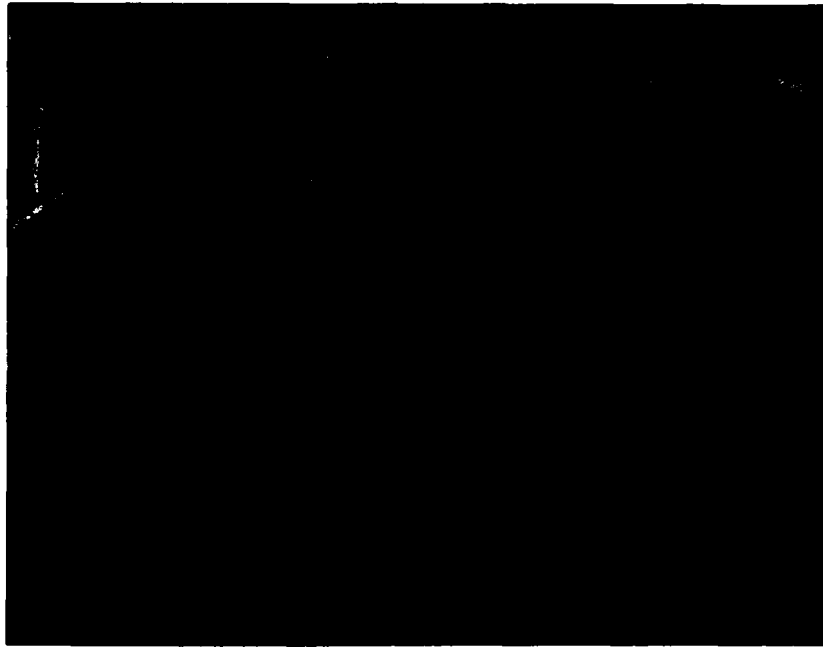


a) Overall View of Specimen Failure Surface

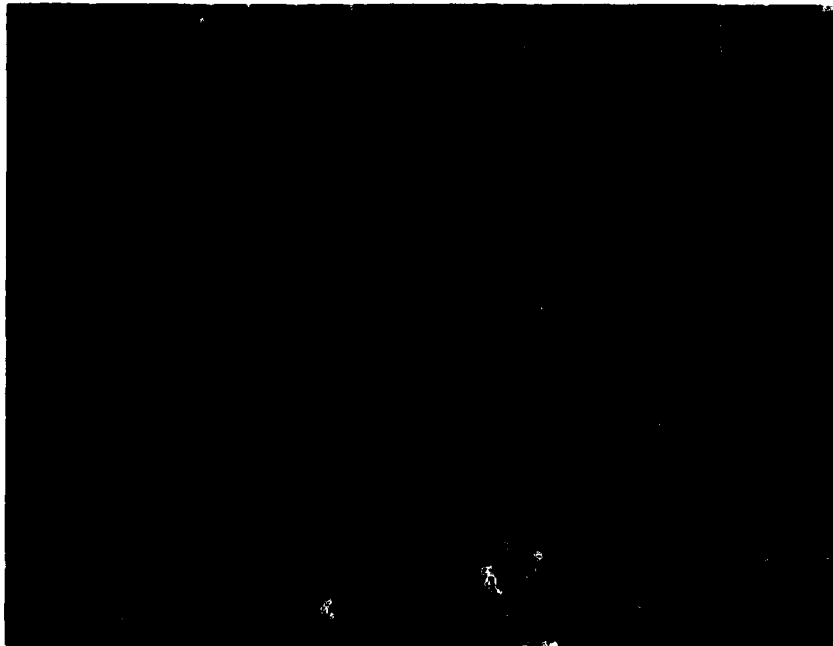


b) Close-up of Failure Initiation Site

Figure 17. Static Tension, Specimen No. ZATL01, Room Temperature Test of Hercules 3501-6 Neat Epoxy Resin (Specimen Failed at 50.3 MPa, i.e., 7.3 ksi).



a) Overall View of Specimen Failure Surface

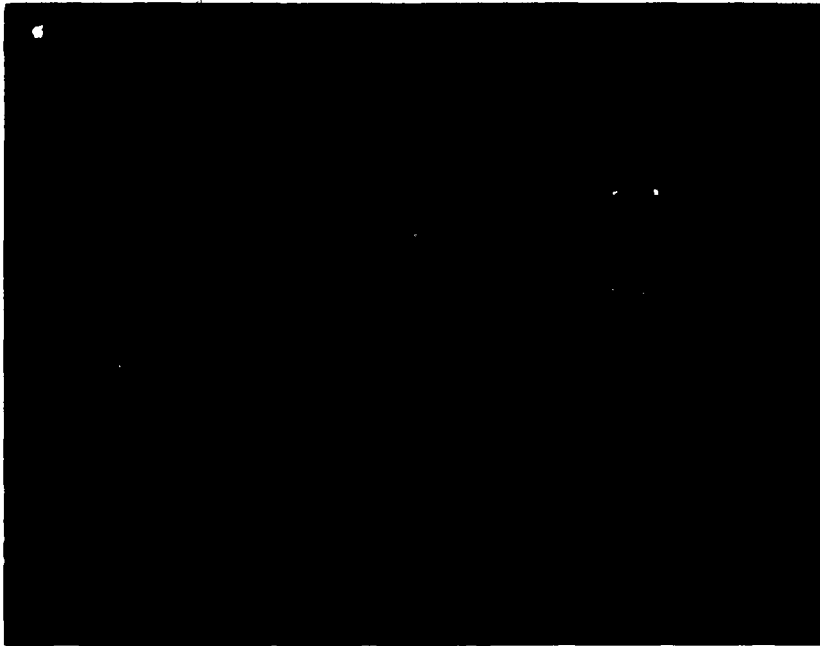


b) Close-up of Failure Initiation Site

Figure 18. Static Tension, Specimen No. ZBTL07, Room Temperature Test of Hercules X4001 Neat Bismaleimide Resin (Specimen Failed at 75.8 MPa, i.e., 11.0 ksi).

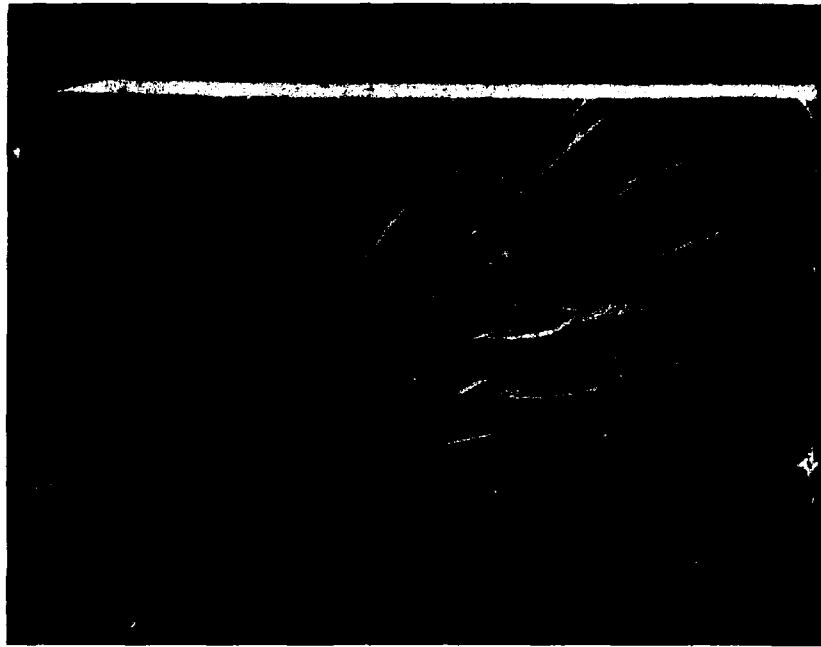


a) Overall View of Specimen Failure Surface



b) Close-up of Failure Initiation Site

Figure 19. Static Tension, Specimen No. ZBTL04, Room Temperature Test of Hercules X4001 Neat Bismaleimide Resin (Specimen Failed at 70.3 MPa, i.e., 10.2 ksi).

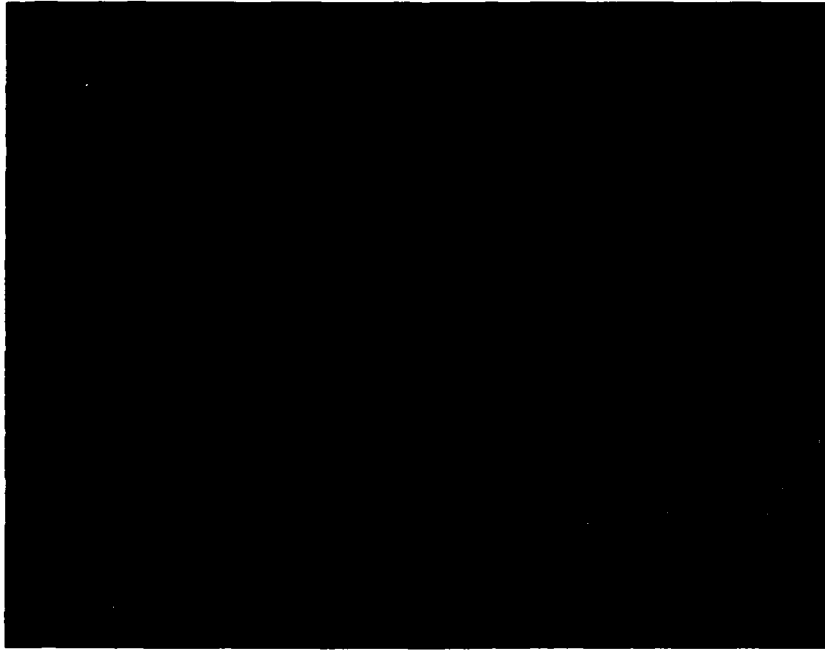


a) Overall View of Specimen Failure Surface

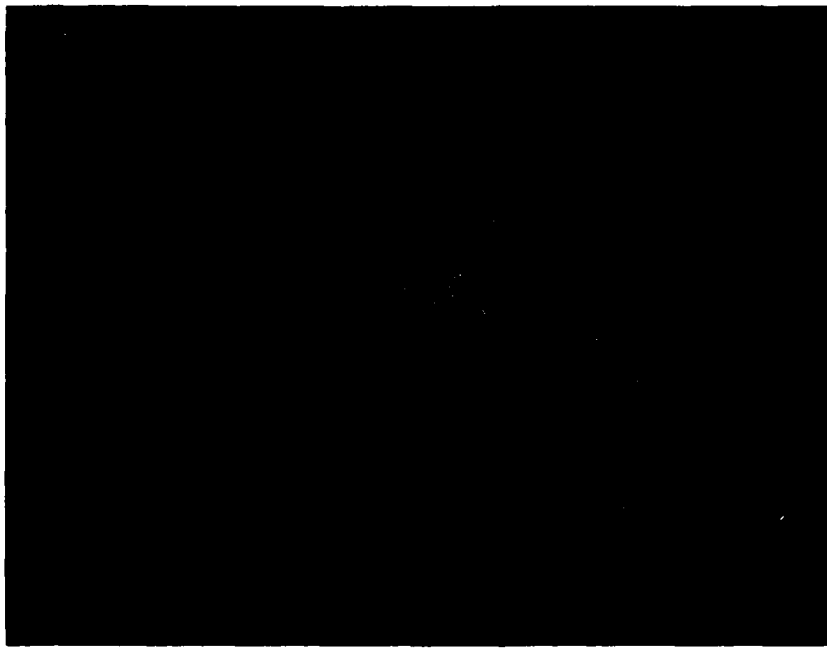


b) Close-up of Failure Initiation Site

Figure 20. Static Tension, Specimen No. ZBTLO3, Room Temperature Test of Hercules X4001 Neat Bismaleimide Resin (Specimen Failed at 66.8 MPa, i.e., 9.7 ksi).

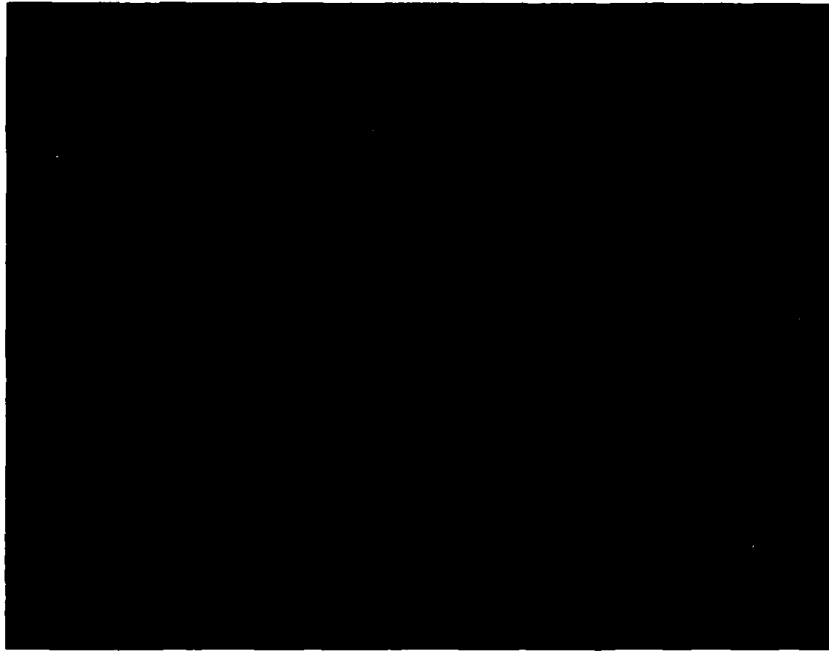


a) Overall View of Specimen Failure Surface

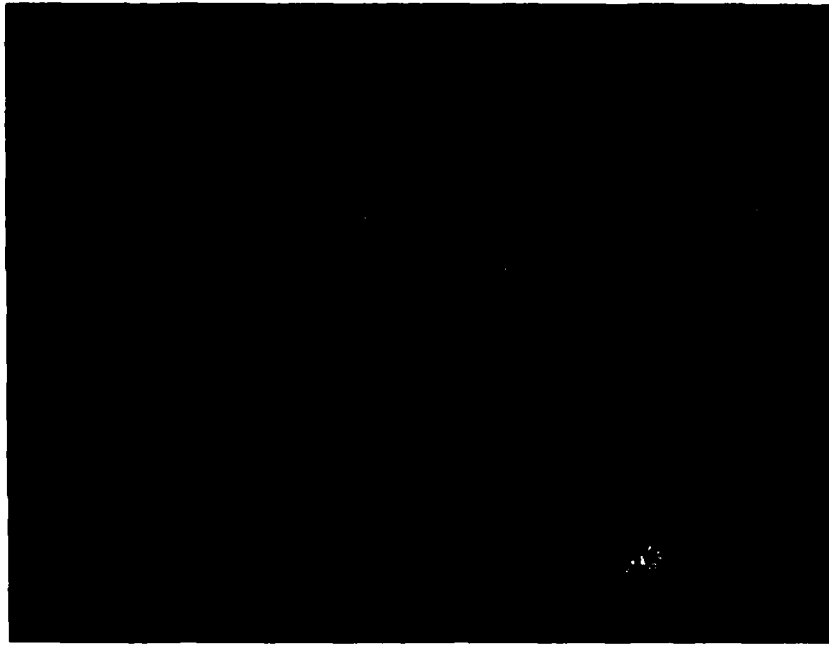


b) Close-up of Failure Initiation Site

Figure 21. Static Tension, Specimen No. ZBTL02, Room Temperature Test of Hercules X4001 Neat Bismaleimide Resin (Specimen Failed at 57.9 MPa, i.e., 8.4 ksi).

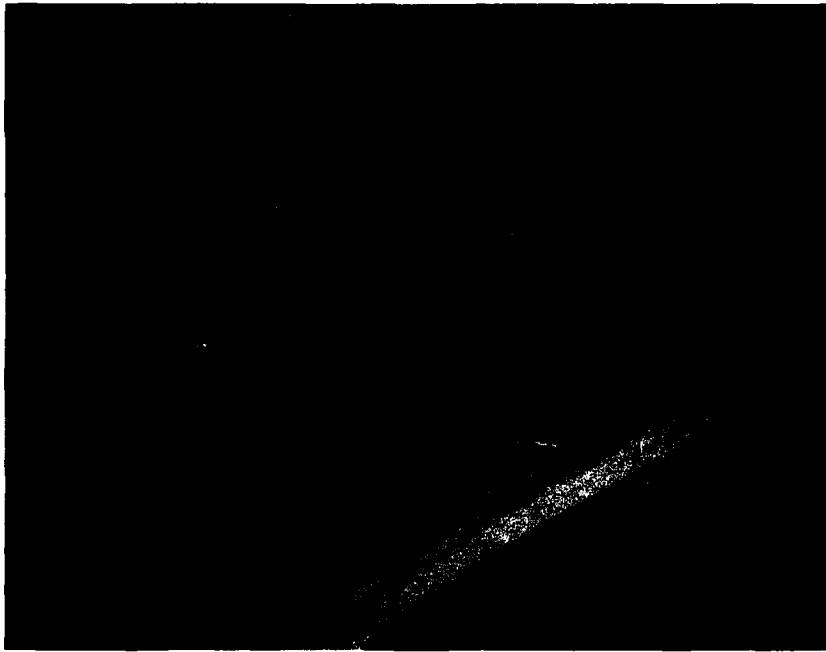


a) Overall View of Specimen Failure Surface



b) Close-up of Failure Initiation Site

Figure 22. Cyclic Tensile Loading, Specimen No. NPTN20, Room Temperature Test of Hercules 3501-6 Neat Epoxy Resin (23,510 Cycles to Failure).



a) Overall View of Specimen Failure Surface



b) Close-up of Failure Initiation Site

Figure 23. Cyclic Torsion Loading, Specimen No. NTRT08, Room Temperature Test of Hercules 3501-6 Neat Epoxy Resin (414,870 Cycles to Failure).

4.3 Summary of SEM Observations

This section will include observations of the fracture surfaces of the SEM photographs presented in Section 4.2 and Appendix C. Speculation as to what these observations indicate in terms of the failure mode of neat resins will be presented in Section 4.4. The observations noted are as follows:

1. The fracture surfaces of specimens tested either statically or cyclically, in tension or torsion, at room temperature or 88°C (190°F), and of either resin system, i.e., Hercules 3501-6 or Hercules X4001, have the same characteristics. The failure mode of the torsion specimens was actually a tensile failure on the plane normal to the direction of maximum principal stress, i.e., on a plane at 45° to the specimen axis.
2. Nearly every specimen observed indicated that the failure initiated at a microscopic void or inclusion, presumed to be the "failure initiation site."
3. All specimens indicated a smooth circular-shaped area around the void or inclusion. In cases where there was not an obvious void or inclusion, careful observation of the center of the smooth circular-shaped area indicated the probable presence of some material anomaly.
4. All specimens exhibited a rough surface bordering the circular-shaped area that extended to the boundaries of the specimen cross section.
5. After studying the static tension test specimen failure surfaces (Figures 14 through 21, included in Section 4.2), a

conclusion can be drawn that the static strength of the neat resin tensile specimens decreased with an increase in the size of the smooth circular-shaped area.

6. For the static tension test specimens, the area of the smooth circular-shaped area increased in size with an increase in size of the failure initiation site.
7. The statically and cyclically loaded specimens exhibited the same failure surface characteristics. However, the smooth circular-shaped area for the cyclically loaded specimens was larger in size than that of the statically loaded specimens.
8. For the cyclically loaded specimens, an increase in the size of the failure initiation site corresponded to a decrease in the number of cycles to failure. However, a low number of cycles to failure also typically inferred a higher cyclic stress.
9. It was suspected that the smooth circular-shaped area might be a penny-shaped crack that propagated from the failure initiation site. If so, during cyclic loading it would be expected that this penny-shaped crack propagated in a start-stop manner. However, SEM observations at higher magnifications offered no evidence of clamshell-type markings to indicate that the smooth circular-shaped area was formed by a propagating, self-arresting penny-shaped crack.

4.4 Interpretation of Specimen Failure Processes

As stated previously, only limited studies have been performed on the failure process of neat resins of the present types. Therefore, this section will include speculations as to the failure process

associated with these materials.

After examining the SEM photographs of the failure surfaces of specimens tested either statically or cyclically, in tension or torsion, at room temperature or 88°C (190°F), and for each type of neat resin, a general conclusion can be drawn. All the specimens failed in the same manner. There is evidence in all the specimen failure surfaces of a failure initiation site, typically a void or inclusion, which is surrounded by a smooth circular-shaped area. This circular-shaped area is surrounded by a very rough surface area that extends to the edges of the cross section of the specimen.

A simple explanation of these failures is that the failure initiation site propagated into a penny-shaped crack, which upon reaching a critical flaw size via stable crack growth, caused catastrophic failure. The actual failure process is undoubtedly much more complex. From observations of the failure surfaces of the fatigue specimens it is concluded that the smooth appearing circular-shaped area probably occurred almost instantaneously during the initial portion of the fracture process.

If this surface area resulted from a controlled (stable) propagation of a penny-shaped crack, it would be reasonable to assume that during fatigue loading the growth of this area would be intermittent. If so, it would be expected that this smooth area would show evidence of this intermittent growth, i.e., clamshell markings. There was no evidence of intermittent crack growth. Additionally, the simple failure process presented implies that plastic deformation may be important during the failure process. The possibility of local plastic deformation is not rejected. However, it appears doubtful that this

mechanism dominated the failure process.

After studying all the failure initiation sites, it is apparent that nearly 50 percent of these sites were flaws that existed before testing was initiated. Typically, these sites were microscopic voids in the resin. For those specimens where an initiation site could not be found, there is evidence of a material anomaly. It can be assumed that the material anomaly propagated into a failure initiation site quite early since cyclically loaded specimens that indicate a failure initiation site in the form of a void had comparable fatigue behavior to those specimens that have a failure initiation site that does not appear to be a void. It is believed that the failure initiation site in all cases either existed prior to testing or developed in the early stages of the testing.

The pre-existence of a failure initiation site also suggests that there was a stress concentration around this site. The magnitude of this stress concentration can be predicted for various assumed flaw geometries. Unfortunately, the exact geometry of the pre-existing flaw is unknown. However, the possible magnitude of the stress concentration can be bounded, and doing so is useful. If the failure initiation site was a spherical void, the stress concentration factor would be 2.05 [10]. For the penny-shaped void, the stress concentration factor approaches infinity. Both of these stress concentration factors assume the material remains elastic. The failure initiation site geometry observed obviously lies between these two extremes. This presents an interesting paradox. It is generally accepted that the materials of the present study are brittle. Therefore, for a spherical void at an applied stress that is approximately 50 percent of the ultimate

strength, the local stress at the flaw would be at the ultimate strength level. If these materials were extremely brittle, it would be expected that the flaw would propagate into a crack in an uncontrolled manner, and that the specimens would fail immediately. The tensile strengths measured for the materials of this study were approximately 6.9 MPa (10 ksi). For a spherical void this would imply that the stress at the void would be about 13.8 MPa (20 ksi). This number is not unreasonable. However, as stated previously, the failure initiation site is not a spherical void. For a penny-shaped failure initiation site, the stress concentration factor approaches infinity, implying that the stresses at the initiation site are infinite. This is totally unreasonable. What this points out is that there must be mechanisms that reduce the stress concentration at the failure initiation site. For metals, the stress relief mechanism is plastic deformation. For polymer materials it is believed that the mechanism is a combination of primarily viscoelastic material response and, secondarily, plastic deformation. Additionally, the above stress concentration factors assume a uniaxial stress state, whereas the stress state around the failure initiation sites is actually triaxial, which would tend to reduce the high uniaxial stresses quoted above.

From the observations of the SEM photographs, and the previous discussion, a possible mode of failure for the two polymer systems of this study can be presented. As stated previously, it is believed that there was a flaw in the test material that existed prior to testing, or formed during the initial stages of testing. This flaw (failure initiation site) is a discontinuity in the specimen which creates a stress concentration. However, the stresses associated with an elastic

stress concentration factor are never achieved due to stress relief induced primarily by viscoelastic material response, and secondarily by plastic deformation. However, the local material on a plane surrounding the failure initiation site, and normal to the direction of the applied load, is being altered by deforming (straining) to achieve the stress relief. At a certain point this material which surrounds a flaw cannot store additional energy. Either the failure of this material leads to total failure, or the fracture incrementally increases in area further, depending on the size of this plane of material and the stress level in the remainder of the specimen. Eventually, total material failure does occur, starting at the failure initiation site and propagating across this fracture plane until a critical flaw size is reached, at which point the specimen fails catastrophically. The region of stable crack growth in this plane is believed to be the smooth circular region evident in all the SEM photographs.

SECTION 5
ANALYSIS OF SPECIMEN FAILURES CAUSED BY
ENVIRONMENTAL CHAMBER MALFUNCTION

5.1 Description of Malfunction

During routine moisture conditioning of a group of the Hercules 3501-6 neat epoxy resin test specimens, the Tenney Benchmaster environmental chamber being used malfunctioned. The moisture injection mechanism failed, causing the chamber environment to go from a hot, humid (75°C, 98 percent relative humidity) to a hot (75°C), dry condition in a then unknown length of time. The approximately 150 Hercules 3501-6 epoxy dog-boned cylindrical specimens in the chamber were fully moisture saturated at the time, and ready for mechanical testing. The same chamber also contained approximately 120 Shell Epon 9101 neat epoxy specimens of the same geometry for use in another program [11], also fully saturated. The chamber failure was known to have occurred sometime between late afternoon and the following morning.

When discovered, approximately half of the Hercules 3501-6 epoxy specimens (73 out of 150) contained large cracks. None of the Shell Epon 9101 epoxy specimens contained visible cracks, and subsequent testing of them indicated no detrimental effects of the chamber failure.

A combined experimental and analytical study was immediately undertaken to determine the conditions that caused the catastrophic failures of the Hercules 3501-6 epoxy resin test specimens.

5.2 Experimental Observations

Both the Hercules 3501-6 and the Shell Epon 9101 epoxy resin specimens involved in the original malfunction had been cast into

dogbone-shaped specimens of circular cross section, and cured per manufacturer's recommendations as follows:

Hercules 3501-6 Epoxy [8]

One-part hot-melt system

Degassed in vacuum desiccator at 107°C for 1 hour

137°C cure for 3 hours

177°C postcure for 3 hours

Shell Epon 9101 Epoxy [11]

100 parts by weight Shell Epon 9101 epoxy

41.5 parts by weight Shell CA9150 curing agent

Degassed in vacuum desiccator at room temperature as required

110°C cure for 3 hours

160°C post cure for 20 minutes

The specimens were approximately 150 mm (6 in) long, with a 7.6 mm (0.3 in) reduced diameter gage length central section 100 mm (2 in) long.

The specimens had been kept in an environmental chamber at a condition of 75°C (167°F) and 98 percent relative humidity for approximately 150 days to attain the fully saturated condition. At the end of 150 days, the specimens were in excellent condition, i.e., without visible cracks.

In the accident reconstruction, an acoustic emission (AE) transducer was mounted on one of the identical specimens and placed in the environmental chamber. The humidifier control of the environmental chamber was then switched off, the temperature being maintained steady at 75°C. The relative humidity inside the chamber was then monitored, readings being taken every 15 minutes from the wet bulb and dry bulb

temperature gauges. The specimens were also visually examined for cracks at 15 minute intervals, through a chamber window.

The x-y recorder of the acoustic emission system recorded some activity at 30 minutes. Another (noninstrumented) Hercules 3501-6 epoxy resin specimen taken out of the chamber for closer visual inspection at the same 30 minute elapsed time exhibited a surface crack along the full length of the specimen. Another surface crack, diagonally opposite the first crack and also running parallel to the specimen axis, formed within the next 15 minutes. For the next 2 hours, these surface cracks propagated radially inward as the relative humidity of the environmental chamber continued to drop. Figure 24 shows the variation of relative humidity of the chamber with time. The recorded acoustic emission signals are reproduced in Figure 25. Figure 26 shows one half of a cracked Hercules 3501-6 specimen.

The experiment was repeated using a Shell Epon 9101 epoxy resin specimen. There were no visible cracks formed at any time throughout the experiment, and no acoustic emission, as anticipated.

5.3 Analysis Approach

Environmental effects, e.g., moisture and temperature, on the structural behavior of polymer and polymer-matrix composites has been a major area of research for several years, and a considerable amount of work has been published [12-16]. However, the effect of a sudden variation of environmental conditions such as that accidentally encountered here had not been specifically addressed. The need for such a study was obvious.

The effect of sudden temperature changes, referred to as "thermal spikes", has been studied by McKague, et al. [17] for graphite/epoxy

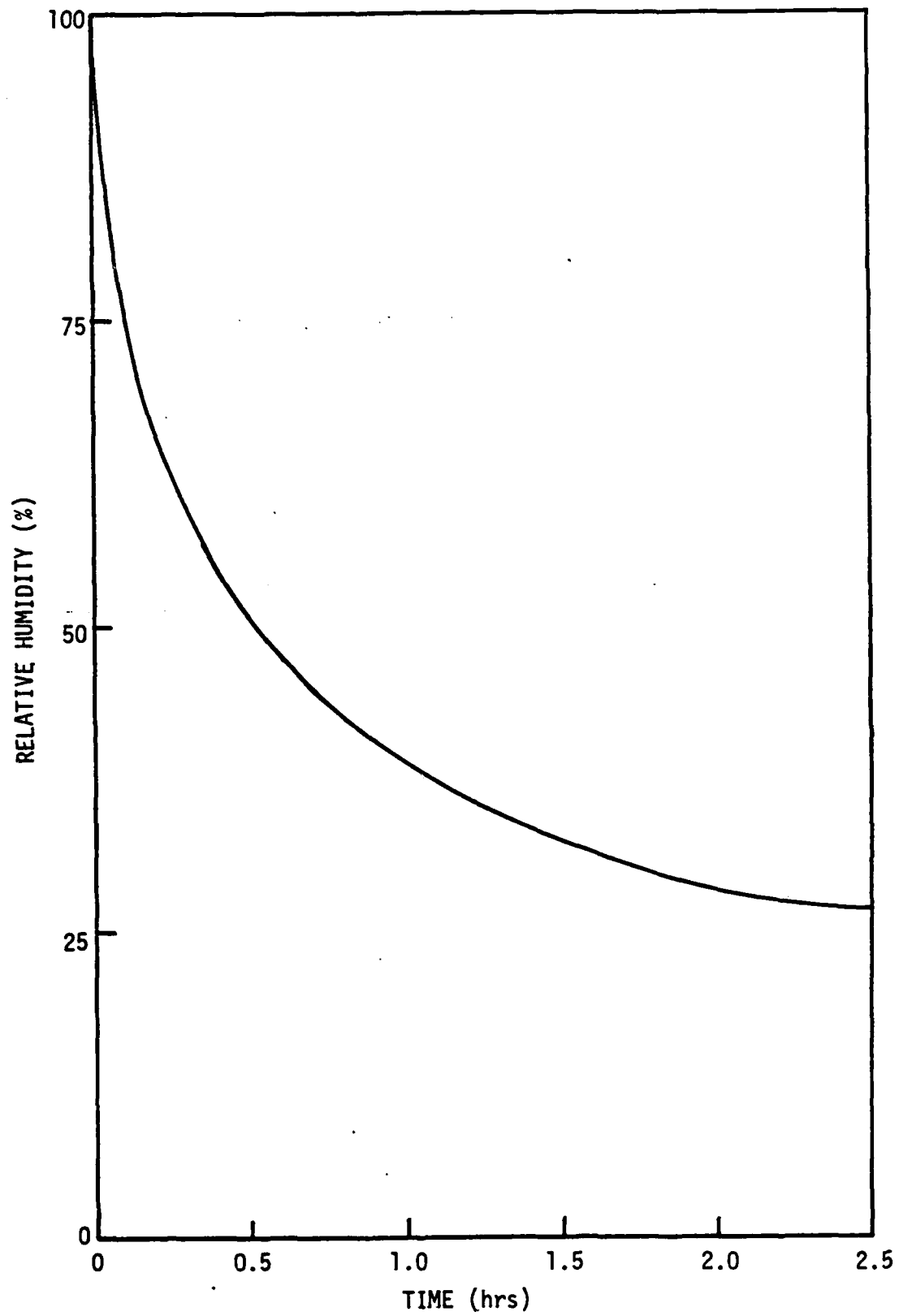


Figure 24. Variation of Relative Humidity of the Environmental Chamber with Time.

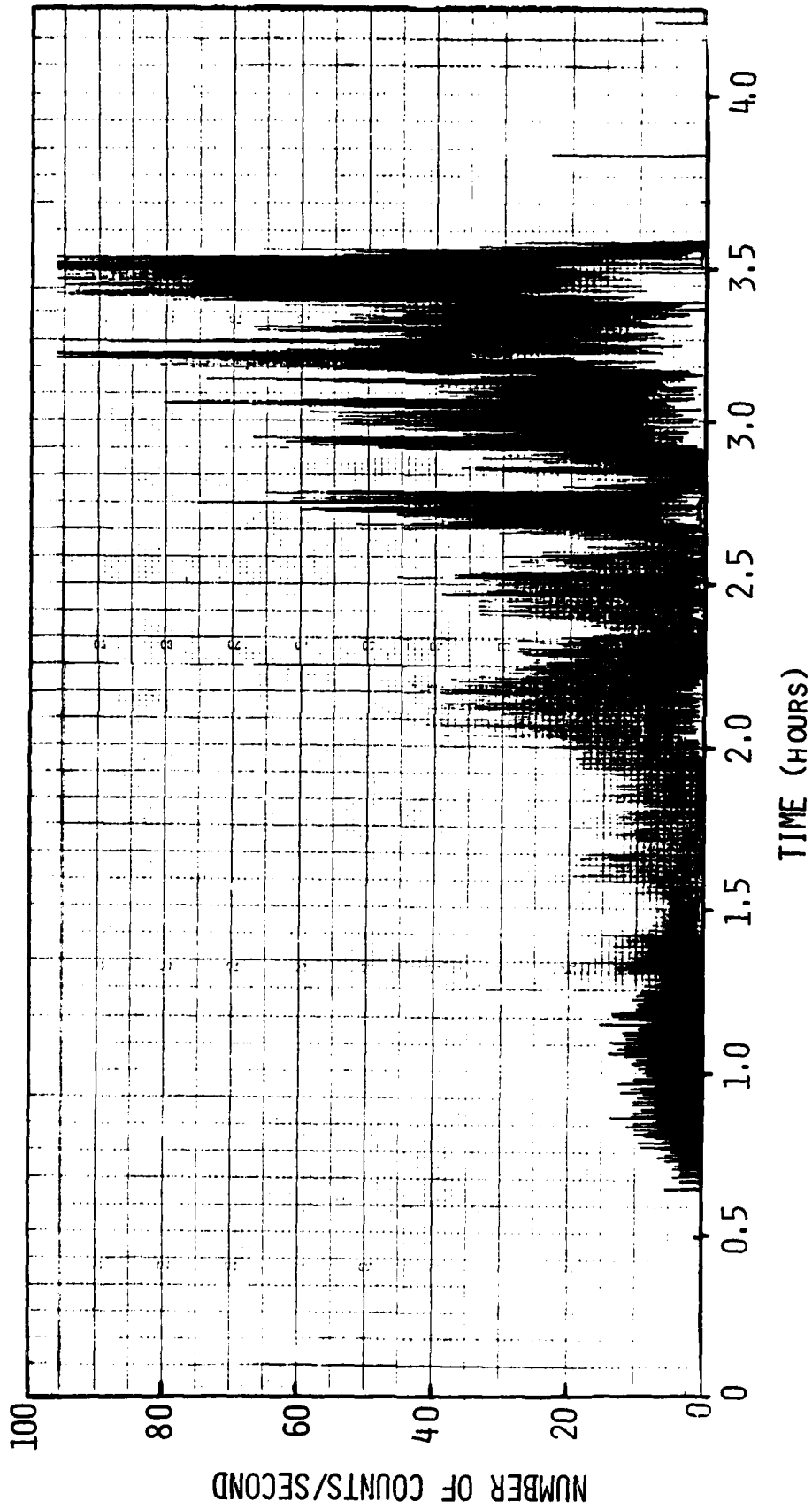


Figure 25. Number of Acoustic Emission Counts per Second vs. Time for the Hercules 3501-6 Neat Epoxy. Subjected to Rapid Dryout from the Moisture-Saturated Condition.



Figure 26. One Half of a Longitudinally Cracked Hercules 3501-6 Epoxy Resin Test Specimen.

laminates, and by Loos and Springer [15] for both unidirectional and quasi-isotropic graphite/epoxy laminates. Even though moisture-induced effects are somewhat analagous to temperature effects, there exist significant differences due to the order of magnitude difference in the thermal conductivity relative to the moisture diffusivity coefficients of typical materials. Because of the low moisture diffusivity coefficients of the polymers and polymer-matrix composites of interest here, any sudden large variation in the moisture environment results in very steep moisture gradients near the material surfaces. These steep moisture gradients, combined with the high moisture expansion coefficients of these materials, may be sufficient to cause severe cracking.

The analytical work involved the prediction of the moisture distribution in the specimen as a function of time for given environmental moisture and temperature conditions, and the evaluation of the induced stresses corresponding to these moisture distributions.

The transient moisture distribution in the specimens was predicted using a combined axisymmetric finite element and finite difference approach, similar to that explained in References [17,18] for transient temperature distributions. An axisymmetric elastoplastic finite element program with hygrothermal loading and crack propagation capabilities [20-22] was used to predict crack initiation and propagation in the specimen.

5.4 Finite Element Analysis

The numerical analysis was carried out in two stages. In the first stage, the transient moisture distributions in the specimens corresponding to the decreasing relative humidity of the environmental

chamber (Figure 24) was obtained using a finite element-finite difference method. The method, which uses axisymmetric finite elements of triangular cross section in space coordinates and a Crank-Nicholson finite difference scheme in the time coordinate, was derived along the lines of an existing transient temperature distribution program [18, 19].

5.4.1 Transient Axisymmetric Moisture Distribution Program (TAXIMD)

The Fickian moisture diffusion equation for an axisymmetric solid is of the form [23]

$$\frac{\partial M}{\partial t} = D_{rr} \frac{\partial^2 M}{\partial r^2} + \frac{D_{rr}}{r} \frac{\partial M}{\partial r} + D_{zz} \frac{\partial^2 M}{\partial z^2} \quad (1)$$

where

M = moisture content (weight percent)

D_{rr}, D_{zz} = moisture diffusion coefficients (mm^2/sec)

The (transient) boundary condition in the present case is the known surface moisture concentration (from Figure 24). That is, at a particular instant of time, $\frac{\partial M}{\partial t}$ at the surface is known. Equation (1), together with the boundary condition, uniquely defines the moisture diffusion problem. However, an alternative formulation is possible with the aid of the calculus of variations [24]. If a functional is written in the form

$$\chi = \frac{1}{2} \int_V [r D_{rr} \left(\frac{\partial M}{\partial r}\right)^2 + r D_{zz} \left(\frac{\partial M}{\partial t}\right)^2 + M \frac{dM}{dt}] dv \quad (2)$$

the necessary and sufficient condition for χ to be a minimum is that it must satisfy the Euler differential equation [24]. The fact that the moisture (or temperature) distribution problem can be reduced to a minimization of some functional in the space domain makes it possible to formulate the problem using the finite element technique.

Assuming the moisture variation in an axisymmetric finite element

of triangular cross section to be linear, the shape functions, element diffusivity matrix, and element capacitance matrix can be defined, as presented in Appendix E. After assembly, the global set of first order linear differential equations is of the form

$$[G] \{M\} + [P] \{\dot{M}\} = 0 \quad (3)$$

where \dot{M} denotes the time rate of change of the moisture content, i.e., $\partial M / \partial t$.

There are a number of numerical methods available to solve this set of linear differential equations, i.e., this initial value problem. The Crank-Nicholson central difference procedure, which is unconditionally stable, was used to solve the differential equations in the computer program TAXIMD developed here for the specific problem at hand. Accordingly, the moisture distribution at time $(t + \Delta t)$ is given as

$$\{M\}_{t+\Delta t} = \{M\}_t + \frac{\Delta t}{z} \frac{\partial M}{\partial t}_{t+\Delta t} + \frac{\partial M}{\partial t}_t \quad (4)$$

The governing Eq. (3), at t and $(t + \Delta t)$, is thus expressed as

$$[G]_t \{M\}_t + [P]_t \left\{ \frac{\partial M}{\partial t} \right\}_t = 0 \quad (5)$$

and

$$[G]_{t+\Delta t} \{M\}_{t+\Delta t} + [P]_{t+\Delta t} \left\{ \frac{\partial M}{\partial t} \right\}_{t+\Delta t} = 0 \quad (6)$$

respectively. From Eq. (4),

$$\left\{ \frac{\partial M}{\partial t} \right\}_{t+\Delta t} = \frac{2}{\Delta t} (\{M\}_{t+\Delta t} - \{M\}_t) - \left\{ \frac{\partial M}{\partial t} \right\}_t \quad (7)$$

Substituting Eq. (7) into Eq. (6),

$$[G]_{t+\Delta t} \{M\}_{t+\Delta t} + [P]_{t+\Delta t} \left(\frac{2}{\Delta t} \{M\}_{t+\Delta t} - \frac{2}{\Delta t} \{M\}_t - \left\{ \frac{\partial M}{\partial t} \right\}_t \right) = 0$$

or

$$([G] + \frac{2}{\Delta t} [P])_{t+\Delta t} \{M\}_{t+\Delta t} - \frac{2}{\Delta t} [P]_{t+\Delta t} \{M\}_t - [P]_{t+\Delta t} \left\{ \frac{\partial M}{\partial t} \right\}_t = 0 \quad (8)$$

Adding Eqs. (5) and (8),

$$(G + \frac{2}{\Delta t} [P])_{t+\Delta t} \{M\}_{t+\Delta t} + [G]_t \{M\}_t - \frac{2}{\Delta t} [P]_{t+\Delta t} \{M\}_t = 0 \quad (9)$$

Knowing the initial moisture condition, the moisture distribution of any

subsequent time can then be solved for.

The moisture diffusivity coefficients assumed for the two resin systems analyzed here are given in Table 2, along with other (room temperature) properties for reference. The initial condition was that corresponding to the moisture saturation state. The surface moisture content corresponding to the relative humidity of the environmental chamber at regular time intervals was the boundary condition at each time interval of the finite difference solution. The finite element grid used to predict the moisture distributions is shown in Figure 27.

Figure 28 shows the moisture distribution for both the Hercules 3501-6 epoxy resin and the Shell Epon 9101 epoxy resin specimens. It can be seen that the Hercules 3501-6 epoxy resin specimen, because of its higher saturation moisture content and lower diffusivity coefficient compared to the Shell Epon 9101 epoxy specimen, exhibited a much higher moisture gradient near the surface.

Table 2
Hercules 3501-6 and Shell Epon 9101 Epoxy Matrix Average Mechanical Properties in the Room Temperature, Dry Condition

<u>Property</u>	<u>Hercules 3501-6 Epoxy [25,26]</u>	<u>Shell Epon 9101/CA 9150 Epoxy [11]</u>
Tensile Modulus, E (GPa)	4.27	3.03
Shear Modulus, G (GPa)	2.14	1.17
Poisson's Ratio, ν	0.34	0.36
Tensile Strength, σ (MPa)	82.7	66.9
Shear Strength, τ (MPa)	84.8	69.0
Coefficient of Thermal Expansion, α ($10^{-6}/^{\circ}\text{C}$)	40.9	30.4
Coefficient of Moisture Expansion, β ($10^{-3}/\%M$)	3.2	2.4
Moisture Diffusivity, D (10^{-7} mm ² /sec)	9.7	29.3

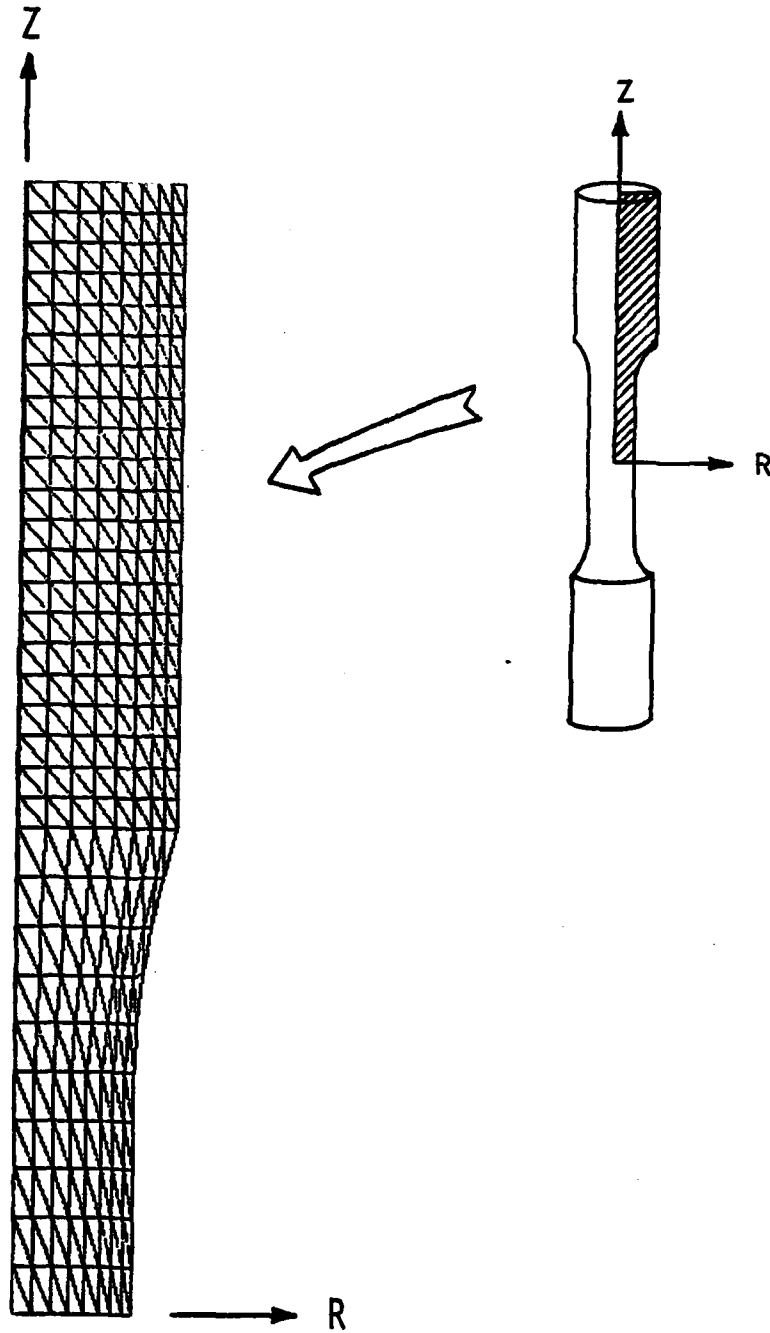


Figure 27. Finite Element Grid Used.

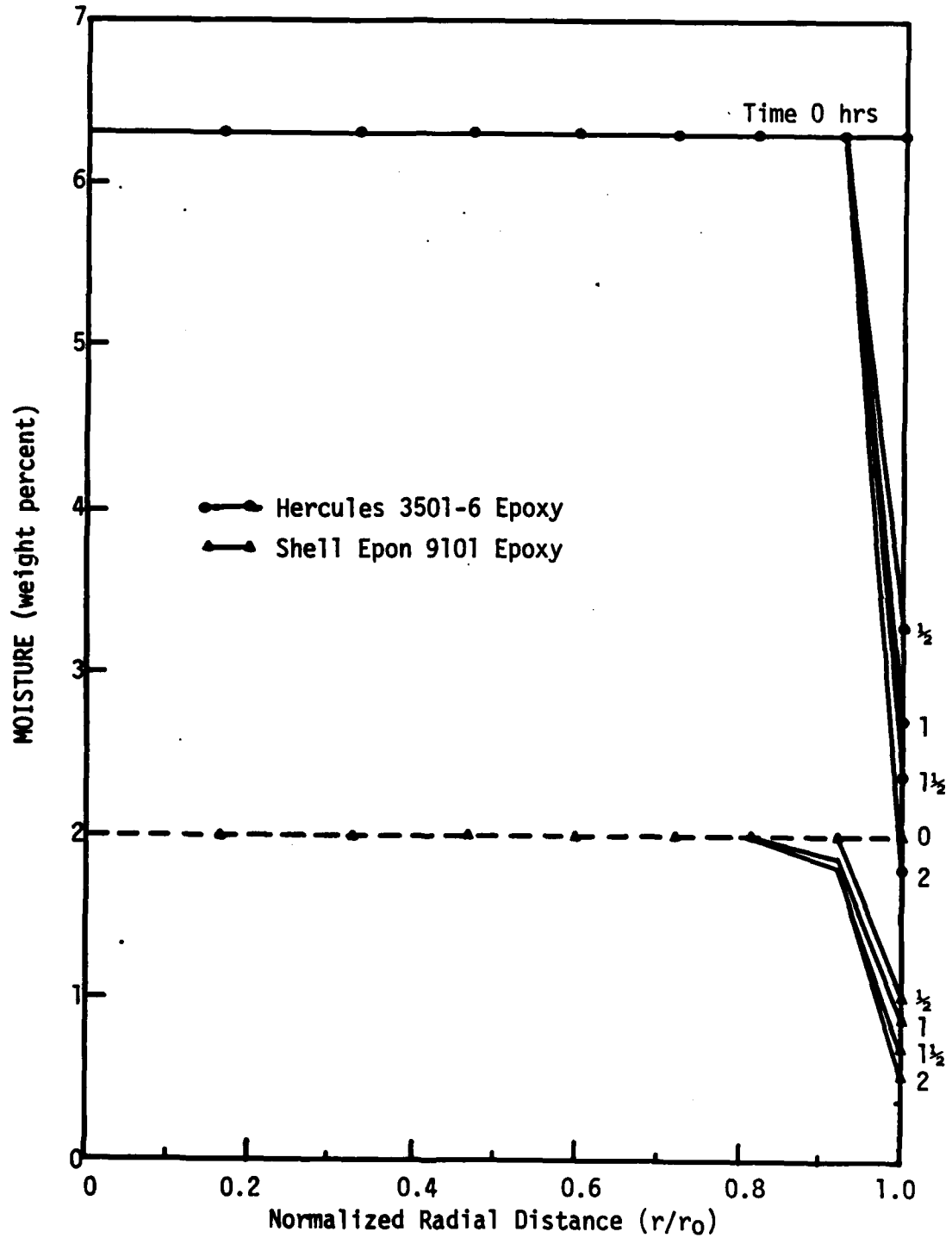


Figure 28. Predicted Moisture Distributions in Two Epoxy Matrix Materials as a Function of Time.

5.4.2 Stress Analysis of Crack Initiation and Propagation

The moisture distribution at regular time intervals (15 minutes) at each finite element node point (Figure 27), obtained from the TAXIMD computer program solution, was used as input to an axisymmetric, elastoplastic, finite element, stress analysis program (EPAC), having hygrothermal loading and crack initiation and propagation capabilities [20-22]. Since EPAC is based on a constant strain triangular axisymmetric finite element, the same finite element grid shown in Figure 27 could be used.

The mechanical properties of the two epoxy resin systems had been previously evaluated by the Composite Materials Research Group (CMRG) as part of various prior research programs [11,25,26].

The material elements at the specimen surface failed when the second increment of moisture distribution was applied (i.e., corresponding to the moisture distribution at the end of 30 minutes). Figure 29 shows the extent of crack initiation and propagation predicted by the EPAC computer program for the Hercules 3501-6 resin specimens at three successive times. There were no failures predicted for the Shell Epon 9101 resin specimens, and of course, none had been observed experimentally.

It should be noted that the surface cracking predicted by the finite element analysis was very similar to that observed both in the original chamber malfunction, and in the subsequent controlled experiments.

5.5 Discussion

The combined analytical and experimental investigation performed here clearly demonstrates that sudden large variations of environmental

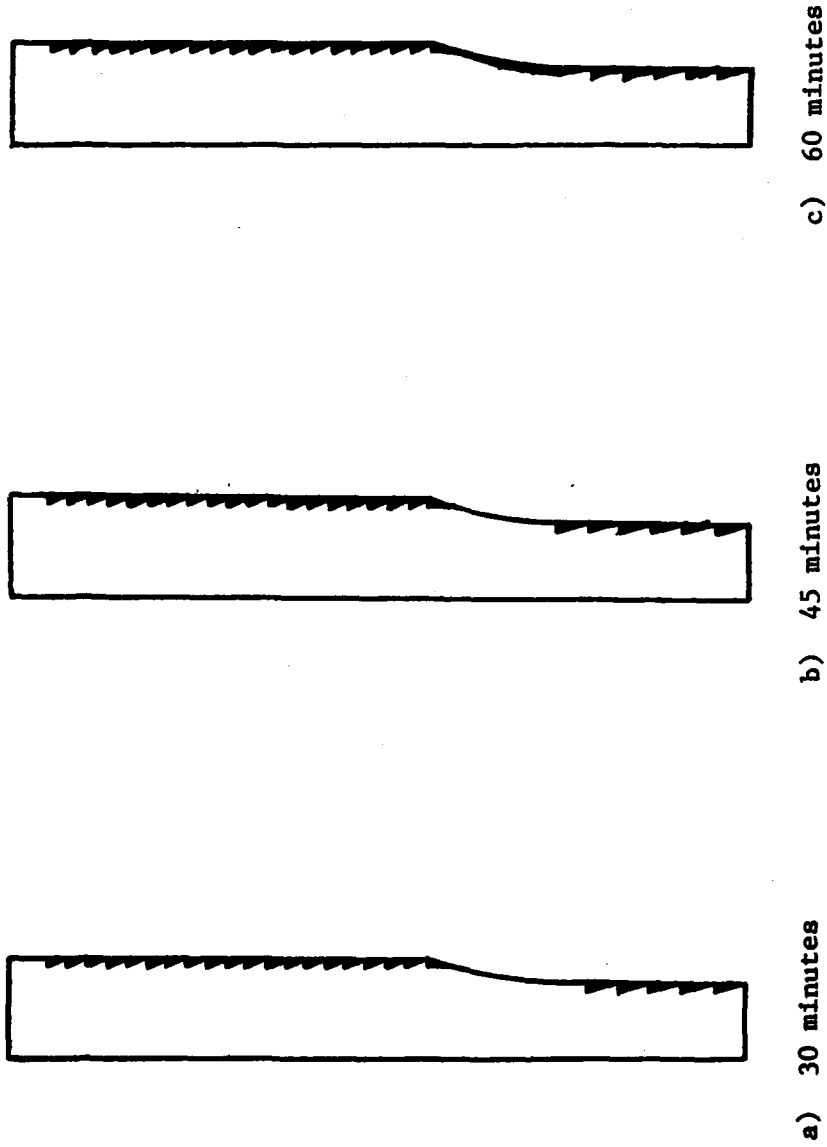


Figure 29. Extent of Crack Initiation and Propagation as a Function of Time Predicted by the Finite Element Analysis for the Hercules 3501-6 Epoxy Matrix Specimen (only one quadrant of specimen shown, see Figure 27).

moisture are highly detrimental to some polymer matrix materials, especially those having lower moisture diffusion coefficients and higher moisture expansion coefficients. This includes the Hercules 3501-6 epoxy used in the present study.

On the other hand, a more ductile (i.e., greater strain to failure) matrix material such as the Shell Epon 9101 epoxy, which also happens to have a higher moisture diffusivity and a lower moisture expansion coefficient (see Table 2), is better able to resist the high stresses (strains) induced by severe moisture gradients.

NADC-83053-60

THIS PAGE INTENTIONALLY LEFT BLANK

SECTION 6

CONCLUSIONS AND SUGGESTIONS FOR FUTURE WORK

6.1 Conclusions

The present study of the fatigue properties of Hercules 3501-6 and X4001 neat epoxy resins resulted in the following conclusions:

1. Methods were developed that allow neat resin to be cast into specimens of consistent quality, at a high production rate.

2. Gripping problems experienced during fatigue testing are now understood and techniques for solving these problems are available.

3. Moisture-induced stresses leading to specimen failure present a very difficult challenge to solve in terms of fatigue testing.

4. In future work involving fatigue testing of neat resin, more specimens per S-N curve than the number (20) included in the present program should be utilized.

5. All fatigue data for both neat resins indicated a knee in the stress versus number of cycles to failure (S-N) curves. Specific reasons for this significant material behavior are unknown at present.

6. The failure mode of the specimens subjected to torsional loads was actually a tensile failure on the plane normal to the direction of maximum principal stress.

7. Failure surfaces of all the specimens indicated the same features. A very carefully controlled study might lead to a qualitative, and perhaps even a quantitative, correlation of the features of the failure surface to the strength of the material.

6.2 Suggestions for Future Work

The major interest of this study was in measuring fatigue

properties of two neat resin materials. While proceeding further in the area of fatigue properties, it is suggested that more basic studies also be conducted. Areas of future interest include the following:

1. While studying the gripping problems outline in Section 2, many different neat resin specimen geometries were utilized. It was noted that a dependence between specimen cross-sectional area and ultimate strength appears to exist. This dependence noted suggests that, as the specimen cross-sectional area becomes smaller, the specimen strength increases. Therefore, a study of specimen size versus strength would be very beneficial in terms of developing specimen designs for future work.

2. By studying the failure surfaces that result from the aforementioned size effect study, a correlation between the failure surface features and the material strength could be developed.

3. It is suggested that future fatigue studies be conducted such that replicate specimens are tested at the same stress level. This would allow a correlation study between the failure surface characteristics and the number of cycles to failure.

4. While conducting the studies outlined above, it is suggested that transparent photoelastic (birefringent) materials be utilized. This will allow observation of the specimen under load. It was noted during this study that there is a random pattern of material anomaly sites that can be observed under polarized light. It is believed that these sites are actually failure initiation sites. If so, observations of these sites could lead to a better understanding of the failure process of neat resin systems.

REFERENCES

1. A.K. Miller, and D.F. Adams, "Micromechanical Aspects of the Environmental Behavior of Composite Materials," Report UWME-DR-707-111-1, Department of Mechanical Engineering, University of Wyoming, January 1977.
2. D.F. Adams, and A.K. Miller, "The Influence of Material Variability on the Predicted Environmental Behavior of Composite Materials," Journal of Engineering Materials and Technology, Vol. 100, No. 1, January 1978, pp. 77-83.
3. A.K. Miller and D.F. Adams, "An Inelastic Micromechanical Analysis of Graphite/Epoxy Composites Subjected to Hygrothermal Cycling," ASTM Conference, "The Environmental Effects on Advanced Composite Materials," Dayton, Ohio, September 1977.
4. D.F. Adams and M.M. Monib, "Moisture Expansion and Thermal Expansion Coefficients of a Polymer-Matrix Composite Material," Proceedings of the Fourth Conference on Fibrous Composites in Structural Design, San Diego, California, November 1978.
5. D.F. Adams, "Temperature- and Moisture-Induced Normal and Shear Stresses at the Fiber/Matrix Interface in Various Composite Materials," Proceedings of the 24th National SAMPE Symposium & Exhibition, San Francisco, California, May 1979.
6. G.C. Grimes and D.F. Adams, "Investigation of Compression Fatigue Properties of Advanced Composites," Northrop Technical Report NOR 79-17, Naval Air Systems Command Contract N00019-77-C-0519, October 1979.
7. D.E. Walrath and D.F. Adams, "Fatigue Behavior of Hercules 3501-6 Epoxy Resin," Report No. NADC-78139-60, Naval Air Development Command Contract NG2289-78-C-0340, January 1980.
8. "Hercules Polymer Matrix Materials Data Sheets," Hercules, Incorporated, Bacchus Works, Magna, Utah, 1982.
9. E.P. Popov, Introduction to Mechanics of Solids, Prentice-Hall, Inc., Englewood Cliffs, New Jersey, 1968.
10. A.P. Boresi, O.M. Sidebottom, F.B. Seely and J.O. Smith, Advanced Mechanics of Materials, 3rd Edition, John Wiley and Sons, New York, 1978.
11. R.S. Zimmerman, D.F. Adams and B.A. Coulter, "Investigation of Moisture Effect Mechanisms in a Unidirectional E-Glass/Epoxy Composite," Report UWME-DR-201-104-1, Department of Mechanical Engineering, University of Wyoming, July 1982.
12. C.H. Shen and G.S. Springer, "Moisture Absorption and Desorption of Composite Materials," Journal of Composite Materials, Vol. 10, No. 1, January 1976, pp. 2-20.

13. F.W. Crossman and A.S.D. Wang, "Stress Field Induced by Transient Moisture Sorption in Finite-Width Composite Laminates," Journal of Composite Materials, Vol. 12, No. 1, January 1978, pp. 2-18.
14. J.R. Vinson, Ed., "Advanced Composite Materials-Environmental Effects," ASTM STP 658, American Society For Testing Materials, Philadelphia, 1978.
15. A.C. Loos and G.S. Springer, "Effects of Thermal Spiking on Graphite-Epoxy Composites," Journal of Composite Materials, Vol. 13, No. 1, January 1979, pp. 17-34.
16. D.E. Walrath and D.F. Adams, "Moisture Absorption Analysis of the Thematic Mapper Graphite/Epoxy Composite Structure," J. R. Vinson, Ed., Modern Developments in Composite Materials and Structures, American Society of Mechanical Engineers, New York, 1979.
17. E.L. McKague, Jr., J.E. Halkias, and J. D. Reynolds, "Moisture in Composites: The Effect of Supersonic Service on Diffusion," Journal of Composite Materials, Vol. 9, No. 1, January 1975, pp. 2-9.
18. J.M. Mahishi and M.V.V. Murthy Chandra, "Transient Heat Conduction in a Composite Nose Cone Due to Aerodynamic Heating," to appear in the Journal of Aeronautical Society of India.
19. J.M. Mahishi, M.V.V. Murthy Chandra and H.V. Lakshminarayana, "Transient Heat Conduction and Thermal Stress Analysis of a Composite Cone Due to Aerodynamic Heating," Report No. NAL-TM-ST-404/183-78, National Aeronautical Laboratory, Bangalore, India, March 1978.
20. D.F. Adams and J.M. Mahishi, "Micromechanical Predictions of Crack Propagation and Fracture Energy in a Single-Fiber Boron/Aluminum Model Composite," Report UWME-DR-201-101-1, Department of Mechanical Engineering, University of Wyoming, Laramie, Wyoming, February 1982.
21. D.F. Adams, "Micromechanical Failure Predictions for Polymer-Matrix Composites," Proceedings of the Fifth Churchill Conference on Deformation, Yield and Fracture of Polymers, University of Cambridge, Cambridge, England, March 1982.
22. J.M. Mahishi and D.F. Adams, "Fracture Behaviour of a Single-Fibre Graphite/Epoxy Model Composite Containing Broken Fibre or Cracked Matrix," Journal of Materials Science, Vol. 18, No. 2, February 1983, pp. 447-456.
23. H.S. Carslaw and J.C. Jaeger, Conduction of Heat in Solids, 2nd Edition, Oxford University Press, London, 1959.
24. H.L. Langhaar, Energy Methods in Applied Mechanics, John Wiley and Sons, New York, 1962.

25. D.A. Crane and D.F. Adams, "Finite Element Micromechanical Analysis of a Unidirectional Composite Including Longitudinal Shear Loading," Report UWME-DR-101-101-1, Department of Mechanical Engineering, University of Wyoming, February 1981.
26. D.S. Cairns and D.F. Adams, "Moisture and Thermal Expansion of Composite Materials," Report UWME-101-104-1, Department of Mechanical Engineering, University of Wyoming, November 1981.

NADC-83053-60

THIS PAGE INTENTIONALLY LEFT BLANK

APPENDICES

NADC-83053-60

THIS PAGE INTENTIONALLY LEFT BLANK

APPENDIX A
NEAT RESIN CASTING TECHNIQUES

THIS PAGE INTENTIONALLY LEFT BLANK

APPENDIX A

NEAT RESIN CASTING TECHNIQUES

The Composite Materials Research Group has been developing casting methods for the fabrication of neat resin specimens for approximately six years. During this present program, previous techniques were refined to the point that it is now a routine process to cast neat resin.

The technique presently utilized is a two-phase process. The first phase entails removing entrapped air and boiling off solvents that are present in the neat resin as it is received from the manufacturer. This phase is performed by placing the neat resin in a heated vacuum oven. The vacuum oven temperature found to work best is 100 to 110°C. This temperature is sufficient to provide a low enough viscosity that entrapped bubbles become mobile. Additionally, at this temperature curing advancement will typically be relatively slow, which allows the time needed to remove all entrapped air and solvents. Once the neat resin is at temperature, a vacuum is drawn above the resin. This vacuum is held until the resin surface is seen to be placid. During the initial stages of the vacuuming, the resin will foam very vigorously. In fact, the molds utilized during the present program were designed to provide a foaming chamber that has approximately 400 times the volume of the neat resin in liquid form. After the first phase of the casting procedure is complete, the neat resin should be free of entrapped air and solvents. This phase is not unlike the initial stages of the cure cycle utilized for laminates. Typically, in the autoclave cure of laminates, there is a low temperature hold utilized for ply

consolidation, which primarily entails removing entrapped air between plies.

The second phase of the resin casting procedure entails removing the mold from the vacuum oven and placing it in an air-circulating oven at a temperature of 135 to 150°C, depending on the neat resin system, for 5 hours. During this time the resin will gel and develop sufficient material properties that it can be removed from the mold. After the neat resin specimens are removed from the mold and inspected, a postcure can be accomplished. The postcure time and temperature are the same as utilized during the manufacture of laminates. The specimens are not postcured in the mold due to the differences in thermal expansion of the resin and the mold, which can cause stress concentrations and even specimen breakage.

All tension specimens were prepared utilizing a box-shaped mold, as shown in Figure A1. The dimensions of this mold are 17.75 cm x 17.75 cm x 22 cm (7.0 in x 7.0 in x 8.6 in). Polished steel dividers are placed on the bottom surface of this mold, separated by small steel spacers as indicated in Figures A1 and A2. All surfaces are sprayed with a fast drying aerosol release agent (Miller-Stephenson MS122 in the present case). This mold is very versatile in that, by changing the thickness of the dividers, specimen thicknesses can be altered. Additionally, specimens of various thicknesses can be fabricated in the same mold at the same time, if desired.

To fabricate round specimens for torsion loading, a single cavity steel mold was utilized. The components of this mold are indicated in Figure A3. These components are assembled and a silicone rubber funnel is placed over the open end of the mold, as indicated in Figure A4.



Figure A1. Steel Box Mold Showing Dividers and Spacers Used to Cast Tension Specimens. (Only Two Sides of the Box are Assembled Here.)

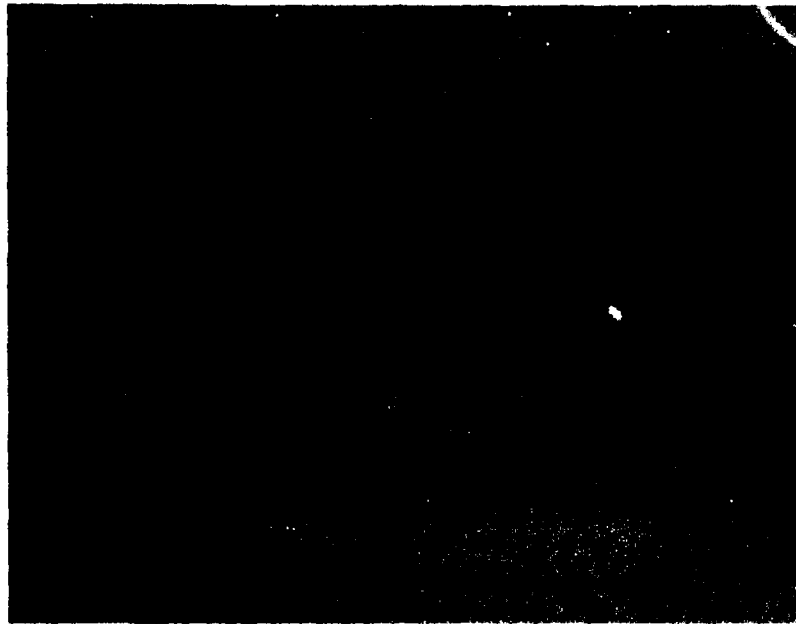


Figure A2. Steel Dividers and Spacers Used in Box Mold of Figure A1 for Fabricating Flat Specimens.

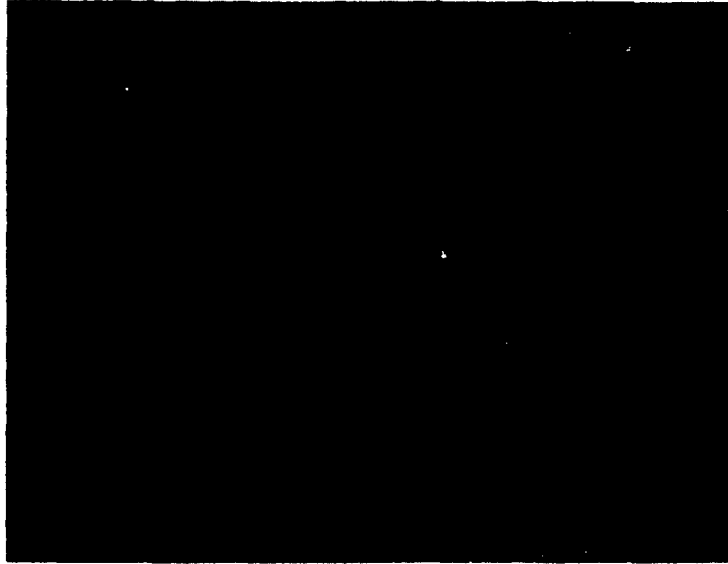


Figure A3. Split Steel Mold Used to Cast Cylindrical Tension Specimens
(mold shown unassembled).



Figure A4. Assembled Cylindrical Specimen Mold, with Silicone Rubber Funnel in Place on Top.

Silicone rubber is utilized for ease of clean up, and to obtain a good seal around the top of the mold.

The cure cycle utilized for fabricating the Hercules 3501-6 and X4001 neat resin specimens is indicated in Table A1. It should be noted in Table A1 that there is a large difference in the postcure times and temperatures.

Table A1

Cure Cycles for Hercules 3501-6 and X4001 Neat Resins [8]

<u>Resin</u>	<u>Vacuum Stage</u>	<u>Gel and Cure Stage</u>	<u>Postcure Stage</u>
3501-6 epoxy	50 min @ 107°C	5 hrs @ 140°C	3 hrs @ 177°C
X4001 bismaleimide	50 min @ 107°C	5 hrs @ 140°C	4 hrs @ 177°C plus 8 hrs @ 204°C

APPENDIX B
INDIVIDUAL TEST RESULTS

THIS PAGE INTENTIONALLY LEFT BLANK

TABLE B-1

TENSILE STATIC AND FATIGUE DATA FOR HERCULES 3501-6
NEAT EPOXY RESIN AT ROOM TEMPERATURE

Test Type	Peak Stress		Cycles to Failure	Elastic Modulus	
	(MPa)	(ksi)		(GPa)	(Msi)
Static	50.3	7.3	1	3.45	0.50
	68.9	10.2	1	3.45	0.50
	62.7	9.9	1	3.58	0.52
	<u>50.3</u>	<u>7.2</u>	1	<u>3.31</u>	<u>0.48</u>
Average	59.4	8.6	1	3.45	0.50
Fatigue (7 hz)	55.2	8.0	8		
	46.9	6.8	40		
	44.1	6.4	70		
	52.4	7.6	130		
	49.6	7.2	220		
	41.3	6.0	600		
	38.6	5.6	960		
	38.6	5.6	1430		
	35.8	5.2	2600		
	41.3	6.0	4830		
	44.1	6.4	5790		
	38.6	5.6	10510		
	37.2	5.4	11380		
	39.9	5.8	14430		
	38.6	5.6	23510		
35.8	5.2	1000000			
33.1	4.8	1000000			
27.6	4.0	1000000			

TABLE B-2

TENSILE STATIC AND FATIGUE DATA FOR HERCULES 3501-6
NEAT EPOXY RESIN AT 88°C

Test Type	Peak Stress		Cycles to Failure	Elastic Modulus	
	(MPa)	(ksi)		(GPa)	(Msi)
Static	55.8	8.1	1	3.65	0.53
	54.5	7.9	1	3.72	0.54
	50.3	7.3	1	3.72	0.54
	55.8	8.1	1	3.65	0.53
	53.1	7.7	1	3.45	0.50
	46.2	6.7	1	3.58	0.52
Average	52.4	7.6		3.58	0.52
Fatigue (7 Hz)	40.7	5.9	120		
	33.8	4.9	300		
	36.5	5.3	410		
	38.6	5.6	490		
	33.8	4.9	520		
	40.7	5.9	560		
	38.6	5.6	680		
	31.0	4.5	820		
	33.8	4.9	1160		
	40.7	5.9	1210		
	35.8	5.2	1710		
	38.6	5.6	2010		
	28.9	4.2	2010		
	31.0	4.5	4830		
	33.8	4.9	5590		
	35.8	5.2	7140		
	27.6	4.0	8480		
	35.8	5.2	9110		
	28.9	4.2	19500		
	27.6	4.0	47000		
26.2	3.8	148330			
26.2	3.8	664820			
26.2	3.8	1000000			
30.3	4.4	1000000			

TABLE B-3

TENSILE STATIC AND FATIGUE DATA FOR HERCULES X4001
NEAT BISMALEIMIDE RESIN AT ROOM TEMPERATURE

Test Type	Peak Stress		Cycles to Failure	Elastic Modulus	
	(MPa)	(ksi)		(GPa)	(Msi)
Static	59.9	8.7	1	3.44	0.50
	75.1	10.9	1	3.65	0.53
	57.2	8.3	1	3.72	0.54
	65.5	9.5	1	3.58	0.52
	70.3	10.2	1	3.65	0.53
	<u>72.3</u>	<u>10.5</u>	1	<u>3.58</u>	<u>0.52</u>
Average	66.2	9.6		3.58	0.52
Fatigue (7 Hz)	58.6	8.5	20		
	58.6	8.5	32		
	58.6	8.5	55		
	62.0	9.0	60		
	55.1	8.0	100		
	62.0	9.0	118		
	55.1	8.0	280		
	62.0	9.0	348		
	51.7	7.5	390		
	55.1	8.0	410		
	46.9	6.8	490		
	48.2	7.0	990		
	49.6	7.2	1960		
	51.7	7.5	1990		
	46.9	6.8	2350		
	46.9	6.8	3630		
	41.4	6.0	7650		
	44.8	6.5	24800		
44.8	6.5	865840			
44.1	6.4	1000000			
43.4	6.3	1000000			

TABLE B-4

TENSILE STATIC AND FATIGUE DATA FOR HERCULES X4001
NEAT BISMALLEIMIDE RESIN AT 88°C

Test Type	Peak Stress		Cycles to Failure	Elastic Modulus	
	(MPa)	(ksi)		(GPa)	(Msi)
Static	57.9	8.4	1	2.83	0.41
	57.9	8.4	1	2.83	0.41
	49.6	7.2	1	2.72	0.40
	61.4	8.9	1	2.41	0.41
	59.9	8.7	1	2.79	0.41
Average	57.2	8.3		2.73	0.40
Fatigue (7 Hz)	49.6	7.2	2		
	49.6	7.2	20		
	34.5	5.0	250		
	41.4	6.0	275		
	38.6	5.6	310		
	41.4	6.0	350		
	44.1	6.4	354		
	44.1	6.4	385		
	44.1	6.4	391		
	38.6	5.6	410		
	37.2	5.4	470		
	37.2	5.4	560		
	38.6	5.6	820		
	34.4	5.0	890		
	31.7	4.6	1210		
	35.8	5.2	1710		
	34.4	5.0	3380		
	37.2	5.4	5200		
	33.1	4.8	5200		
	33.1	4.8	6280		
	35.8	5.2	8130		
	35.8	5.2	10150		
	35.8	5.2	58110		
33.1	4.8	70160			
31.7	4.6	123210			
30.3	4.4	1000000			
31.7	4.6	1000000			
33.1	4.8	1000000			
34.4	5.0	1000000			
34.4	5.0	1000000			

TABLE B-5

TORSION STATIC AND FATIGUE DATA FOR HERCULES 3501-6
NEAT EPOXY RESIN AT ROOM TEMPERATURE

Test Type	Peak Stress		Cycles to Failure	Shear Modulus	
	(MPa)	(ksi)		(GPa)	(Msi)
Static	55.8	8.1	1	1.7	0.25
	70.3	10.2	1	1.8	0.26
	83.4	12.1	1	1.8	0.26
	71.7	10.4	1	1.8	0.26
	<u>99.7</u>	<u>14.4</u>	1	<u>1.8</u>	<u>0.26</u>
Average	78.6	11.4		1.8	0.26
Fatigue (3 Hz)	62.1	9.0	3		
	55.2	8.0	76		
	51.7	7.5	100		
	58.6	8.5	111		
	58.6	8.5	183		
	48.3	7.0	560		
	37.9	5.5	1250		
	41.4	6.0	5700		
	37.9	5.5	7220		
	44.8	6.5	16401		
	37.9	5.5	45070		
	44.8	6.5	184440		
	34.5	5.0	414890		
	31.0	4.5	1000000		

TABLE B-6

TORSION STATIC AND FATIGUE DATA FOR HERCULES 3501-6
NEAT EPOXY RESIN AT 88°C

Test Type	Peak Stress		Cycles to Failure	Shear Modulus	
	(MPa)	(ksi)		(GPa)	(Msi)
Static	95.1	13.8	1	1.79	0.26
	98.5	14.3	1	1.65	0.24
	84.8	12.3	1	1.79	0.26
	67.5	9.8	1	1.79	0.26
	83.4	12.1	1	1.65	0.24
Average	86.1	12.1		1.72	0.25
Fatigue (3 Hz)	52.4	7.6	2		
	49.0	6.8	10		
	41.3	6.0	1160		
	49.6	7.2	1280		
	49.0	6.8	1420		
	40.0	5.8	3850		
	35.8	5.2	4840		
	37.2	5.4	4990		
	38.6	5.6	10250		
	35.8	5.2	16230		
	38.6	5.6	40600		
	34.5	5.0	65510		
	35.8	5.2	216280		
	33.1	4.8	446060		
34.5	5.0	489120			
30.3	4.4	1000000			

TABLE B-7

TORSION STATIC AND FATIGUE DATA FOR HERCULES X4001
NEAT BISMALEIMIDE RESIN AT ROOM TEMPERATURE

Test Type	Peak Stress		Cycles to Failure	Shear Modulus	
	(MPa)	(ksi)		(GPa)	(Msi)
Static	69.6	10.1	1	1.86	0.27
	79.2	11.5	1	1.65	0.24
	63.4	9.2	1	*	*
	71.7	10.4	1	*	*
	95.1	13.8	1	*	*
Average	75.8	11.0		1.76	0.26
Fatigue (3 Hz)	68.9	10.0	2		
	58.6	8.5	50		
	62.0	9.0	80		
	55.1	8.0	87		
	65.5	9.5	150		
	65.5	9.5	515		
	48.2	7.0	820		
	48.2	7.0	1280		
	58.6	8.5	2092		
	51.7	7.5	2950		
	55.1	8.0	7100		
	48.2	7.0	15250		
	51.7	7.5	59740		
	41.3	6.0	297440		
	37.9	5.5	1000000		
41.3	6.0	1000000			
44.8	6.5	1000000			
51.7	7.5	1000000			

* Data not available

TABLE B-8

TORSION STATIC AND FATIGUE DATA FOR HERCULES X4001
NEAT BISMALLEIMIDE RESIN AT 88°C

Test Type	Peak Stress (MPa)	Stress (ksi)	Cycles to Failure	Elastic Modulus (GPa)	Elastic Modulus (Msi)
Static	70.9	10.3	1	1.38	0.20
	66.8	9.7	1	1.31	0.19
	66.1	9.6	1	1.45	0.21
	68.9	10.0	1	*	*
Average	68.9	9.9		1.38	0.20
Fatigue	41.3	6.0	10		
	38.0	5.5	60		
	37.2	5.4	370		
	41.3	6.0	1806		
	33.1	4.8	2010		
	35.6	5.1	2740		
	39.3	5.7	4620		
	36.4	5.2	7280		
	37.2	5.4	27070		
	36.0	5.2	28100		
	37.2	5.4	28180		
	39.3	5.7	303670		
	35.1	5.1	528400		
	37.2	5.4	822760		
	35.1	5.1	1000000		
33.1	4.8	1000000			
39.3	5.7	1000000			

*Data not available

APPENDIX C

ROTOMETER DESCRIPTION AND THEORY OF OPERATION

NADC-83053-60

THIS PAGE INTENTIONALLY LEFT BLANK

APPENDIX C

ROTOMETER DESCRIPTION AND THEORY OF OPERATION

A test method to measure the shear modulus of the Hercules 3501-6 and X4001 neat resin materials was developed which utilized a torsional loading, two cams attached to a round specimen, and four Linearly Variable Differential Transformers (LVDT) to translate the angular motion of the torsion test into a linear motion in the LVDT and hence a signal for use by the data acquisition system. Four LVDT are required to cancel out any specimen eccentricity effects. The locations of the two cams define the gage length of the round specimen.

A photograph showing the basic arrangement is presented in Figure C1. The cams are only cut over an angle of 90° , leaving 270° of circular surface area for the opposing LVDT to ride on. The top cam allows the cancellation of any twist sensed by the lower cam that originates outside the gage section of the specimen. By subtracting the upper LVDT pair signal from the lower LVDT pair signal, the difference in rotation between the two can be derived by knowing that the cam gives a 0.1" rise in 90° of rotation. The opposing LVDT are electrically wired to cancel any eccentricity that may be introduced by cam placement or any other source. If an eccentricity does exist, as one LVDT moves out, the opposing LVDT will move in, and the electrical signals cancel. Daytronic signal conditioners then take the upper and lower pair LVDT signals and subtract them before the resultant voltage is transmitted to the computer data acquisition system used for recording the test data.

Calibrating the LVDT to account for the 0.1" rise for 90° rotation allows the calculation of shear stress τ , shear strain γ , and shear

modulus G by use of the following equations [9,10]:

$$G = \frac{\tau}{\gamma}, \tau = \frac{Tr}{J}$$

$$\gamma = r \frac{d\theta}{dL} = \frac{r\Delta\theta}{L} = \frac{Tr}{JG}$$

and

$$G = \frac{TL}{J\theta}$$

where T = applied torque

θ = angle of twist

J = polar moment of inertia

L = specimen gage length

r = specimen radius

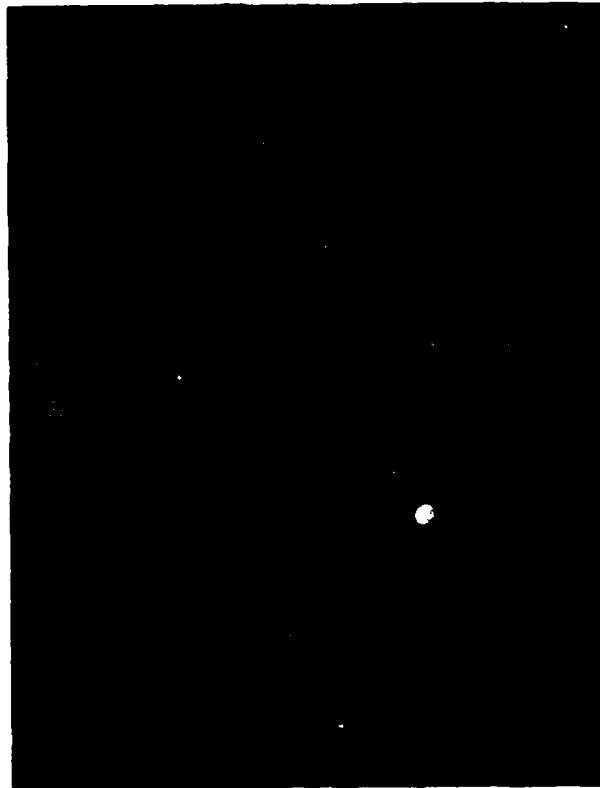


Figure C1. Rotometer apparatus for measuring shear strain on round specimens with two cams and four LVDT.

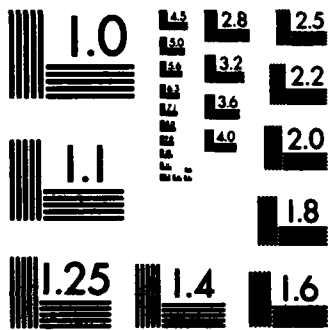
AD-A135 076

A STUDY OF POLYMER MATRIX FATIGUE PROPERTIES(U) WYOMING 2/2
UNIV LARAMIE DEPT OF MECHANICAL ENGINEERING
E M ODOM ET AL. JUN 83 UWME-DR-301-103-1 NADC-83053-60
N62269-80-C-0278 F/G 11/4

UNCLASSIFIED

NL





MICROCOPY RESOLUTION TEST CHART
NATIONAL BUREAU OF STANDARDS-1963-A

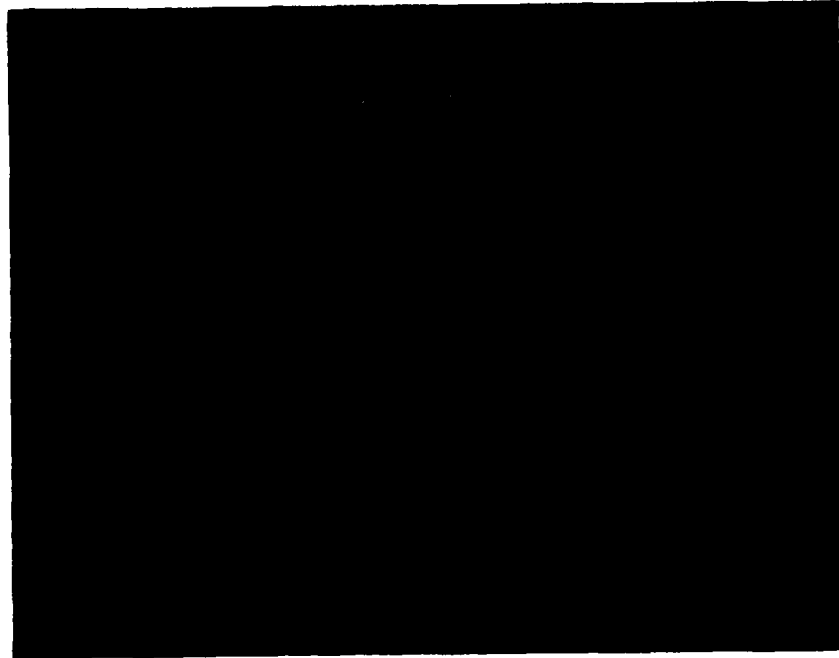
NADC-83053-60

APPENDIX D

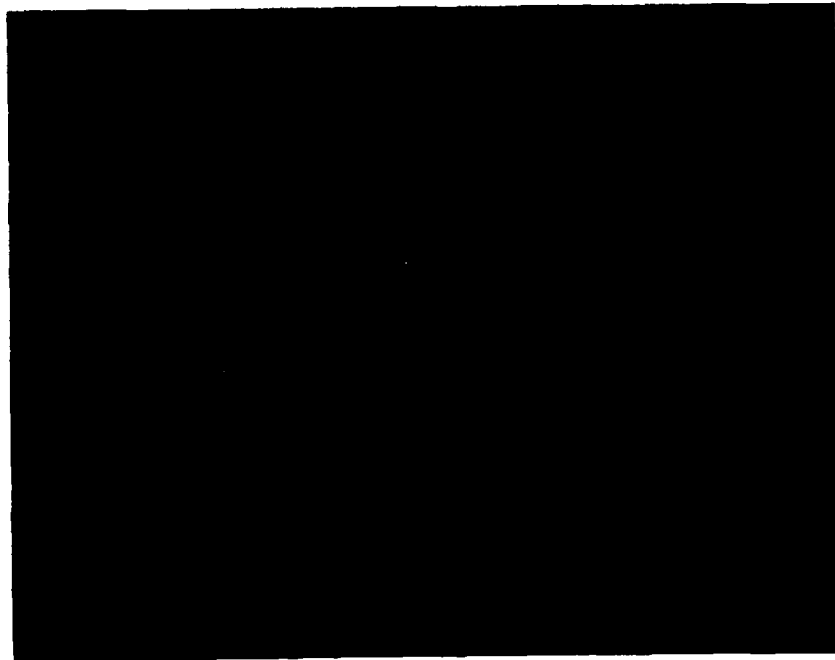
SEM PHOTOGRAPHS OF SPECIMEN FAILURE SURFACES

NADC-83053-60

THIS PAGE INTENTIONALLY LEFT BLANK

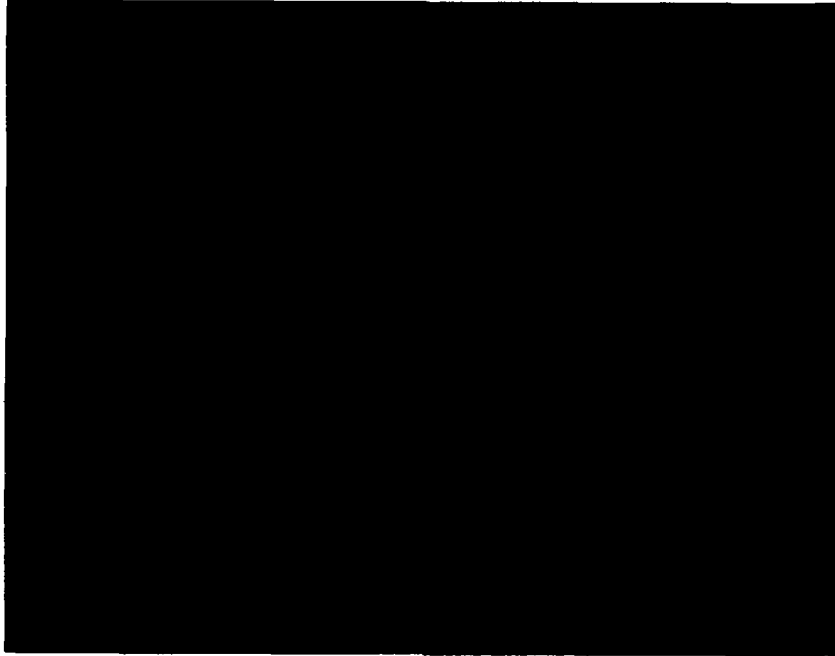


a) Overall View of Specimen Failure Surface



b) Close-up of Failure Initiation Site

Figure D1. Tension Fatigue, Specimen No. NTPN19, Room Temperature Test of Hercules 3501-6 Neat Epoxy Resin (Specimen Cycled at 38.6 MPa, i.e., 5.6 ksi, Failed at 10,510 Cycles).



a) Overall View of Specimen Failure Surface

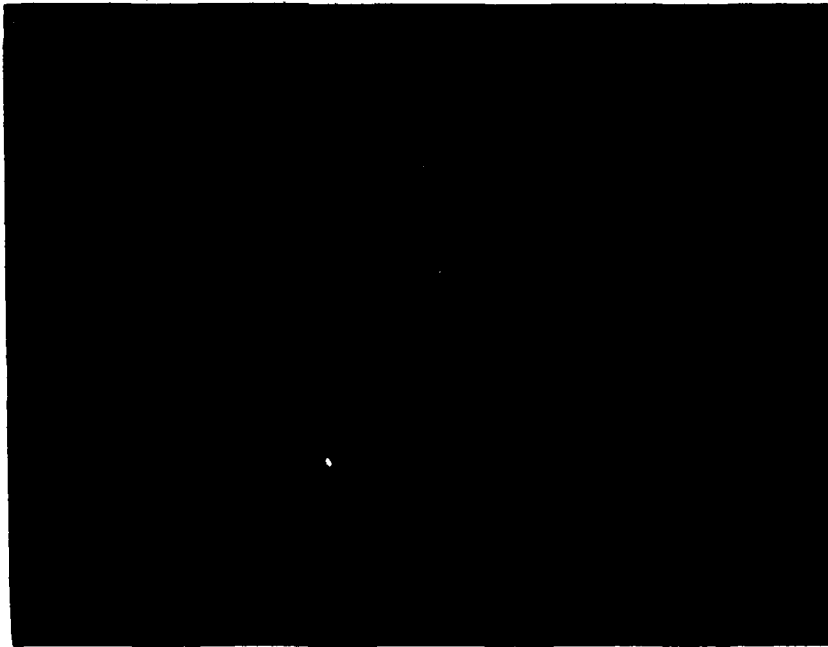


b) Close-up of Failure Initiation Site

Figure D2. Tension Fatigue, Specimen No. NTPN15, Room Temperature Test of Hercules 3501-6 Neat Epoxy Resin (Specimen Cycled at 41.3 MPa, i.e., 60 ksi, Failed at 4,830 Cycles).



a) Overall View of Specimen Failure Surface



b) Close-up of Failure Initiation Site

Figure D3. Tension Fatigue, Specimen No. NTPN16, Room Temperature Test of Hercules 3501-6 Neat Epoxy Resin (Specimen Cycled at 38.6 MPa, i.e., 5.6 ksi, Failed at 1,430 Cycles).

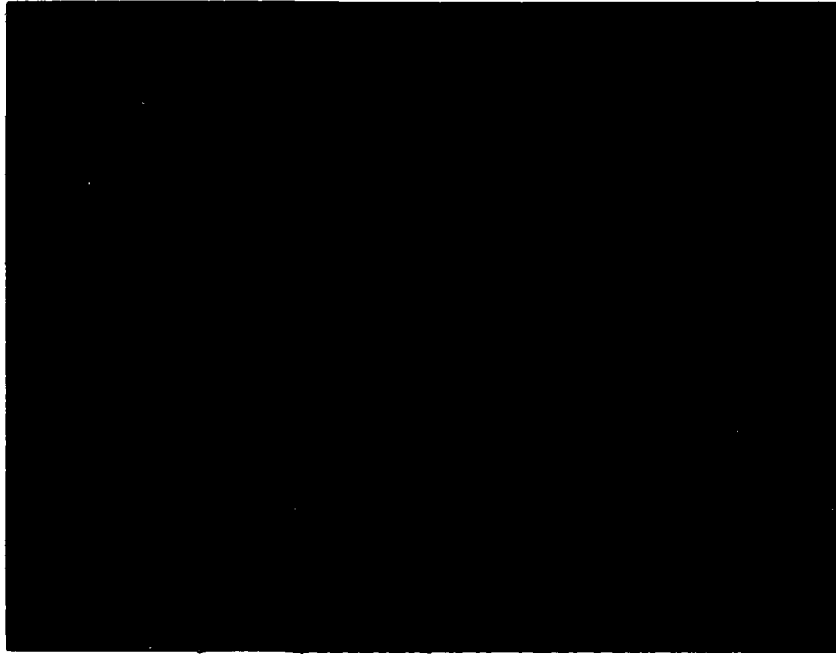


a) Overall View of Specimen Failure Surface



b) Close-up of Failure Initiation Site

Figure D4. Tension Fatigue, Specimen No. NTON07, 88°C Test of Hercules 3501-6 Neat Epoxy Resin (Specimen Cycled at 26.2 MPa, i.e., 3.8 ksi, Failed at 148,330 Cycles).

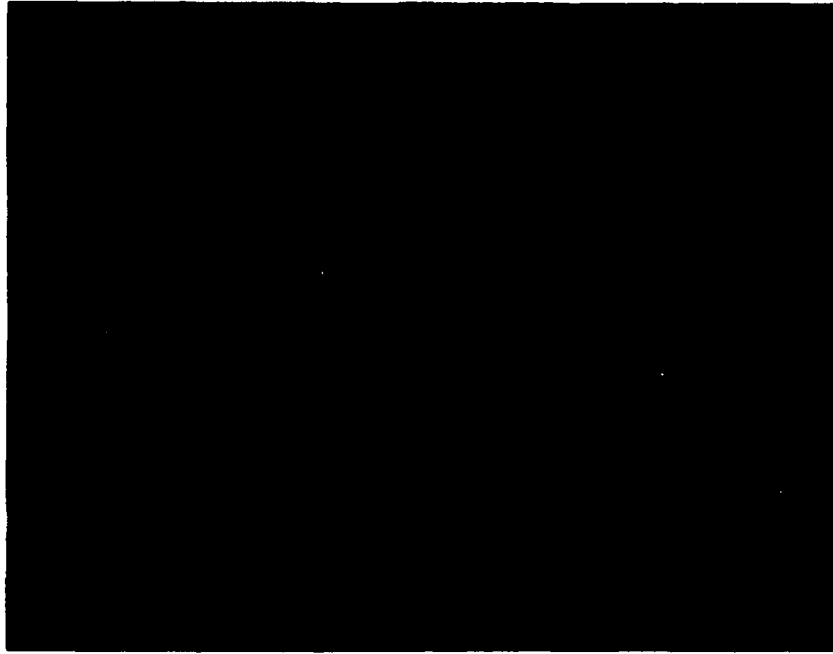


a) Overall View of Specimen Failure Surface



b) Close-up of Failure Initiation Site

Figure D5. Tension Fatigue, Specimen No. NTON09, 88°C Test of Hercules 3501-6 Neat Epoxy Resin (Specimen Cycled at 27.6 MPa, i.e., 4.0 ksi, Failed at 47,000 Cycles).



a) Overall View of Specimen Failure Surface



b) Close-up of Failure Initiation Site

Figure D6. Tension Fatigue, Specimen No. NTON06, 88°C Test of Hercules 3501-6 Neat Epoxy Resin (Specimen Cycled at 38.6 MPa, i.e., 5.6 ksi, Failed at 2010 Cycles).



a) Overall View of Specimen Failure Surface



b) Close-up of Failure Initiation Site

Figure D7. Tension Fatigue, Specimen No. NTON14, 88°C Test of Hercules 3501-6 Neat Epoxy Resin (Specimen Cycled at 33.8 MPa, i.e., 4.9 ksi, Failed at 300 Cycles).



a) Overall View of Specimen Failure Surface

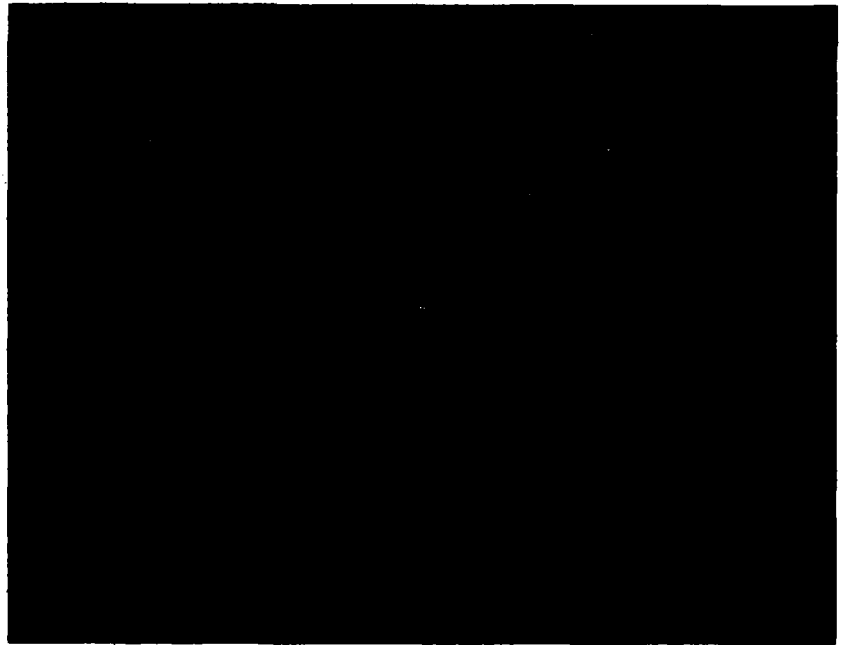


b) Close-up of Failure Initiation Site

Figure D8. Tension Fatigue, Specimen No. NTFX08, Room Temperature Test of Hercules X4001 Neat Bismaleimide Resin (Specimen was Cycled at 41.4 MPa, i.e., 6.0 ksi, Failed at 7,650 Cycles).

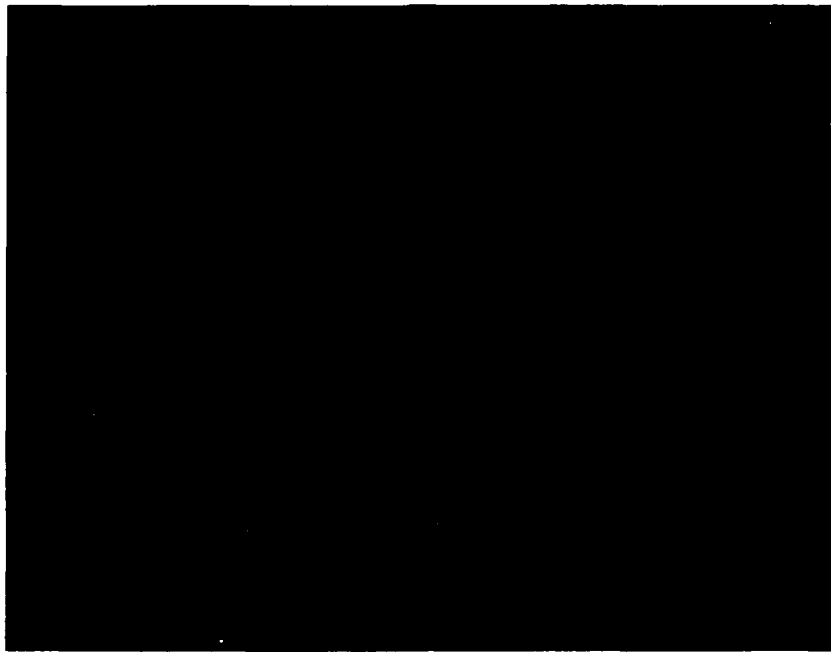


a) Overall View of Specimen Failure Surface



b) Close-up of Failure Initiation Site

Figure D9. Tension Fatigue, Specimen No. NTFX02, Room Temperature Test of Hercules X4001 Neat Bismaleimide Resin (Specimen Cycled at 49.6 MPa, i.e., 6.8 ksi, Failed at 1,960 Cycles).

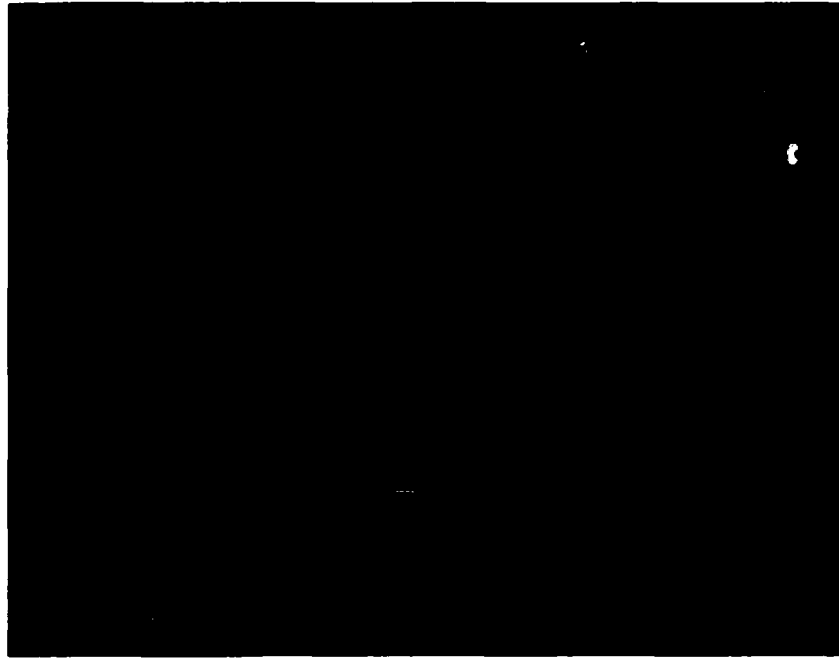


a) Overall View of Specimen Failure Surface



b) Close-up of Failure Initiation Site

Figure D10. Tension Fatigue, Specimen No. NTFX03, Room Temperature Test of Hercules X4001 Neat Bismaleimide Resin (Specimen Cycled at 55.1 MPa, i.e., 8.0 ksi, Failed at 280 Cycles).



a) Overall View of Specimen Failure Surface

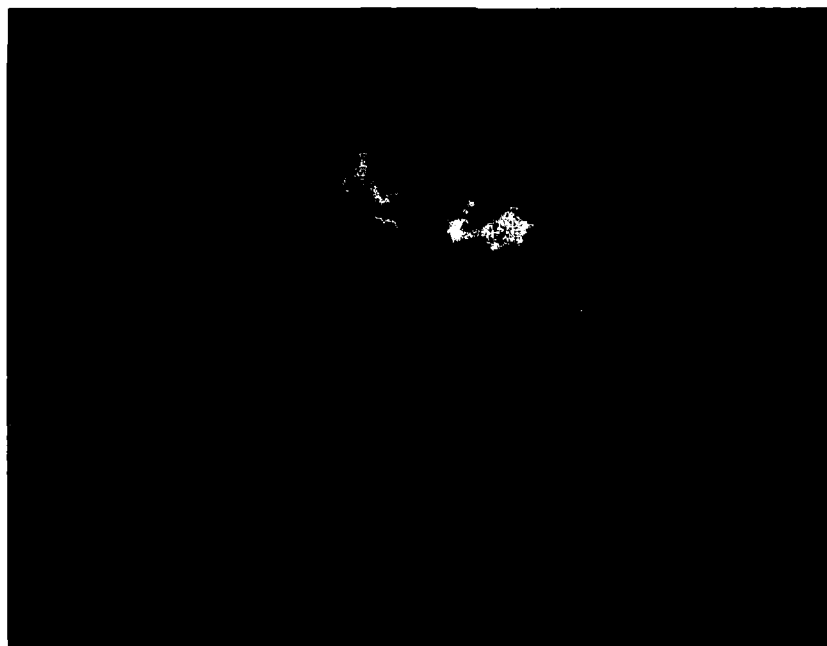


b) Close-up of Failure Initiation Site

Figure D11. Tension Fatigue, Specimen No. NTXN13, 88°C Test of Hercules X4001 Neat Bismaleimide Resin (Specimen Cycled at 35.8 MPa, i.e., 5.2 ksi, Failed at 1,710 Cycles).

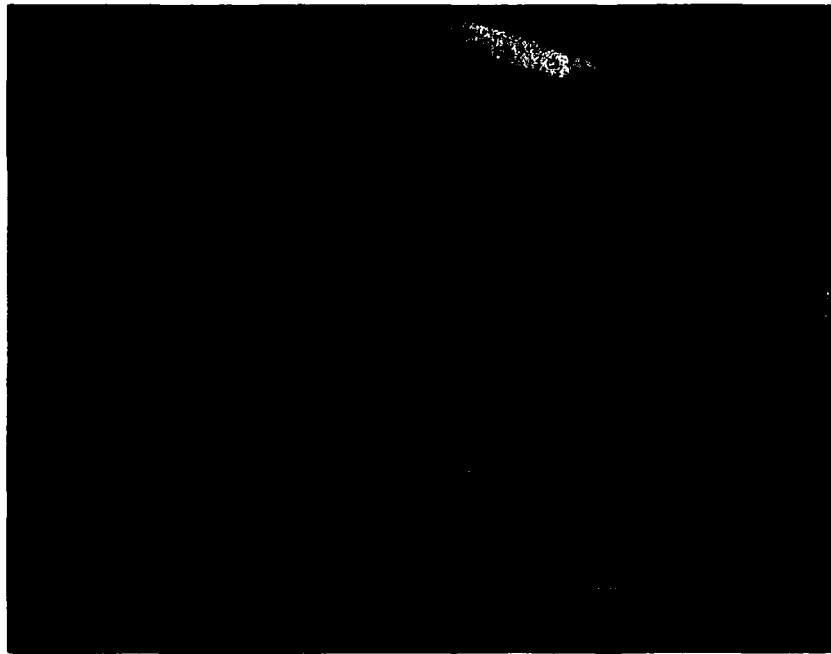


a) Overall View of Specimen Failure Surface

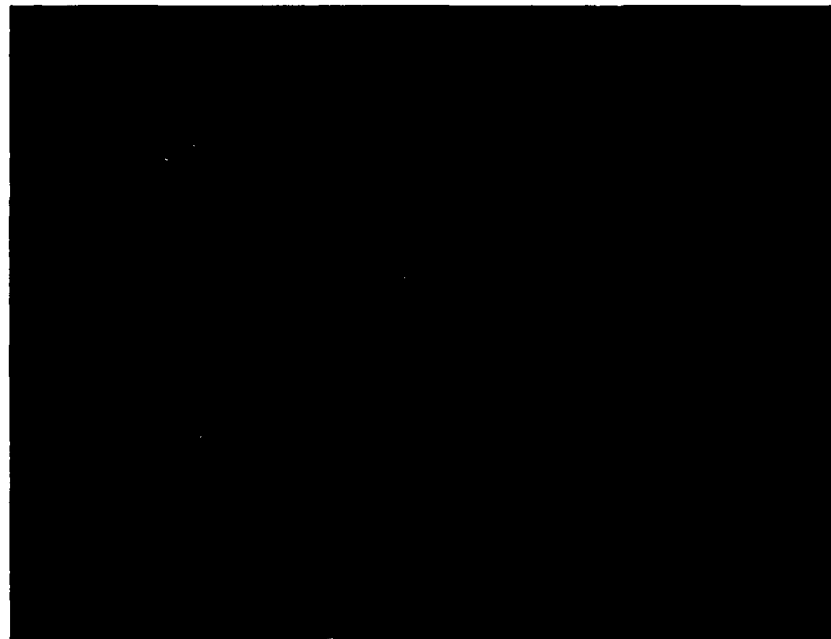


b) Close-up of Failure Initiation Site

Figure D12. Tension Fatigue, Specimen No. NTXN28, 88°C Test of Hercules X4001 Neat Bismaleimide Resin (Specimen Cycled at 49.6 MPa, i.e., 7.2 ksi, Failed at 20 Cycles).

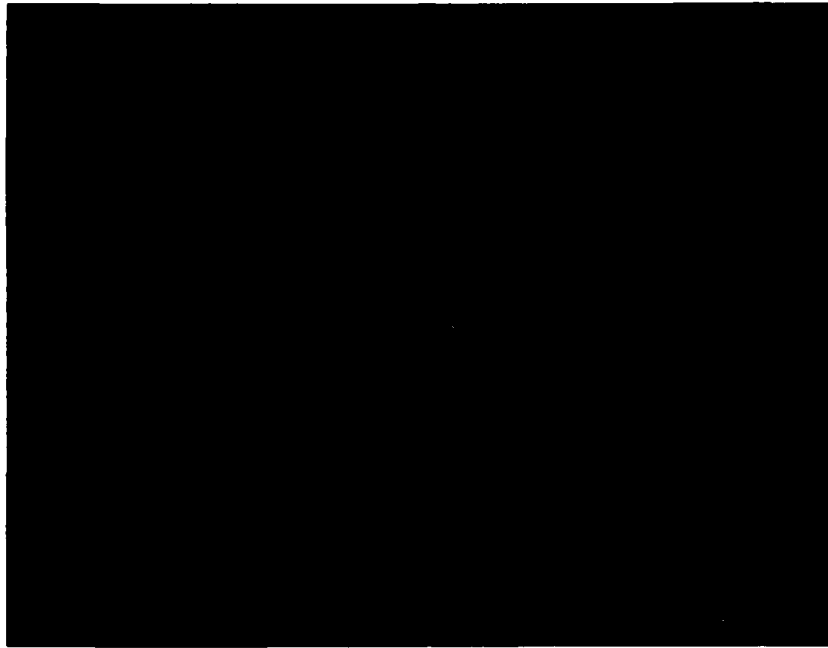


a) Overall View of Specimen Failure Surface

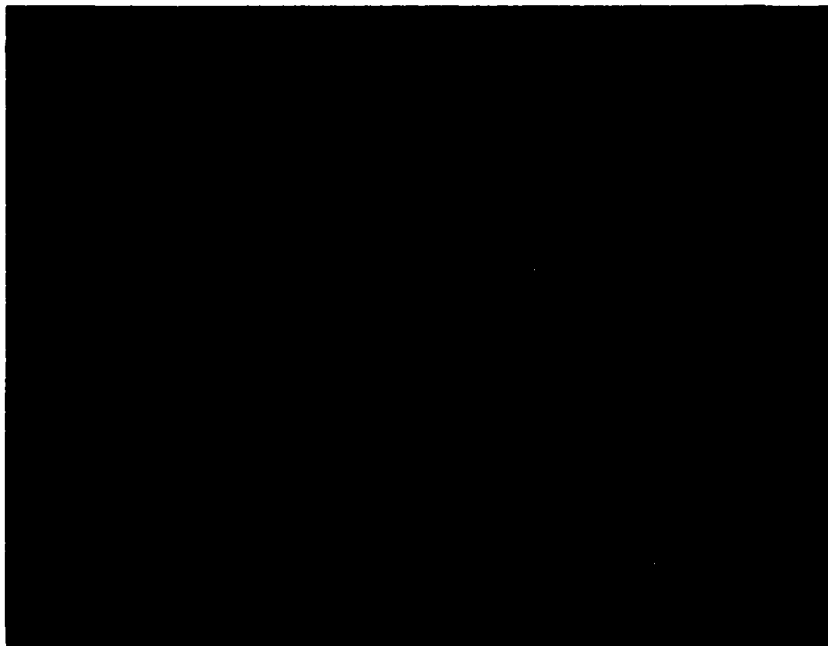


b) Close-up of Failure Initiation Site

Figure D13. Torsion Fatigue, Specimen No. NTRT17, Room Temperature Test of Hercules 3501-6 Neat Epoxy Resin (Specimen Cycled at 44.8 MPa, i.e., 6.5 ksi, Failed at 184,440 Cycles).



a) Overall View of Specimen Failure Surface

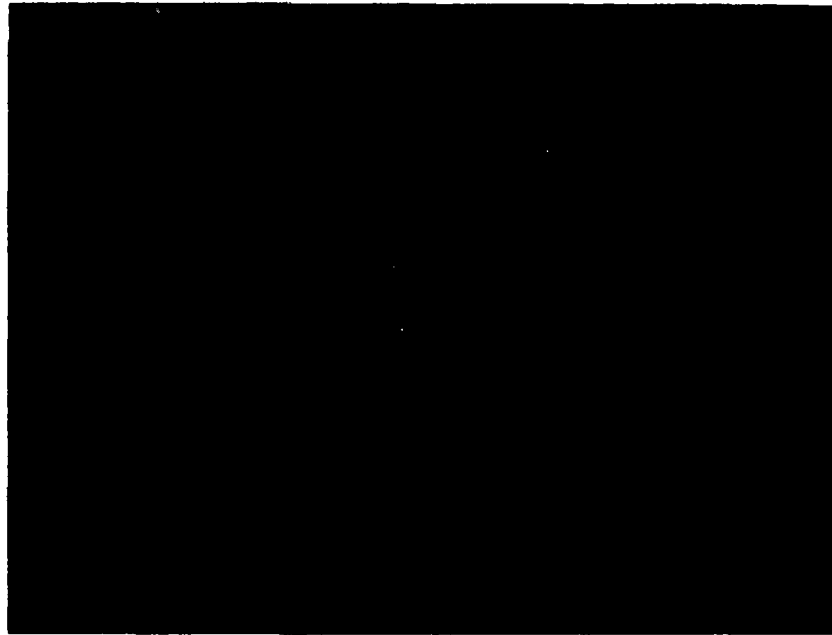


b) Close-up of Failure Initiation Site

Figure D14. Torsion Fatigue, Specimen No. NTRT12, Room Temperature Test of Hercules 3501-6 Neat Epoxy Resin (Specimen Cycled at 37.9 MPa, i.e., 5.5 ksi, Failed at 45,070 Cycles).



a) Overall View of Specimen Failure Surface



b) Close-up of Failure Initiation Site

Figure D15. Torsion Fatigue, Specimen No. NTRT01, Room Temperature Test of Hercules 3501-6 Neat Epoxy Resin (Specimen Cycled at 62.1 MPa, i.e., 9.0 ksi, Failed at 3 Cycles).



a) Overall View of Specimen Failure Surface



b) Close-up of Failure Initiation Site

Figure D16. Torsion Fatigue, Specimen No. NTTB06 88°C Test of Hercules 3501-6 Neat Epoxy Resin (Specimen Cycled at 38.6 MPa, i.e., 5.6 ksi, Failed at 40,600 Cycles).

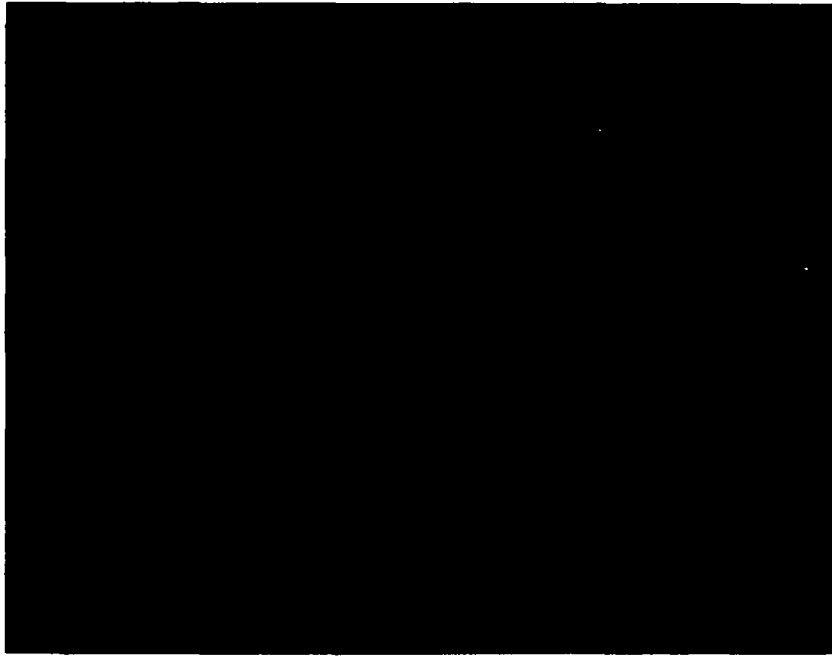


a) Overall View of Specimen Failure Surface



b) Close-up of Failure Initiation Site

Figure D17. Torsion Fatigue, Specimen No. NTTB01, 88°C Test of Hercules 3501-6 Neat Epoxy Resin (Specimen Cycled at 38.6 MPa, i.e., 5.6 ksi, Failed at 10,250 Cycles).



a) Overall View of Specimen Failure Surface



b) Close-up of Failure Initiation Site

Figure D18. Torsion Fatigue, Specimen No. NTTB03, 88°C Test of Hercules 3501-6 Neat Epoxy Resin (Specimen Cycled at 41.3 MPa, i.e., 6.0 ksi, Failed at 1,160 Cycles).



a) Overall View of Specimen Failure Surface

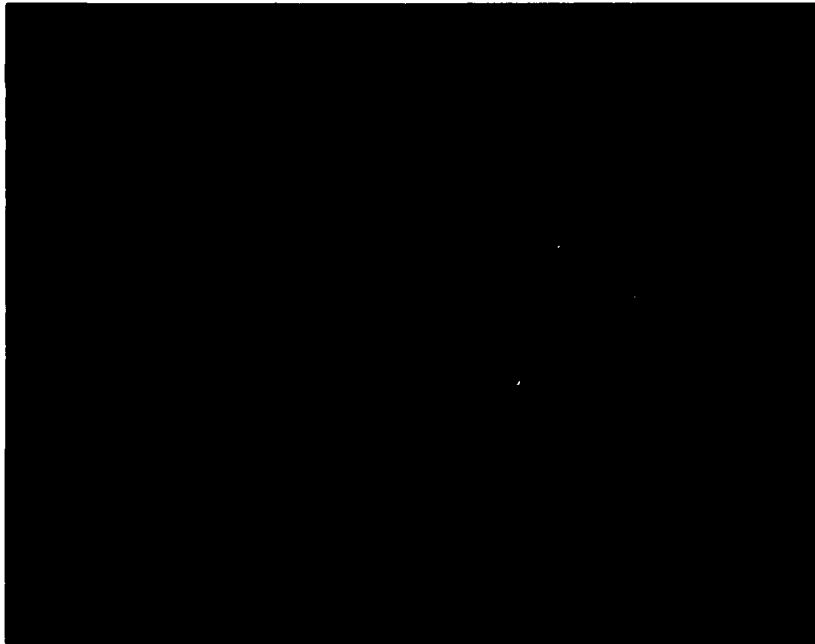


b) Close-up of Failure Initiation Site

Figure D19. Torsion Fatigue, Specimen No. NTTX01, Room Temperature Test of Hercules X4001 Neat Bismaleimide Resin (Specimen Cycled at 41.3 MPa, i.e., 6.0 ksi, Failed at 297,440 Cycles).



a) Overall View of Specimen Failure Surface



b) Close-up of Failure Initiation Site

Figure D20. Torsion Fatigue, Specimen No. NTTX23, Room Temperature Test of Hercules X4001 Neat Bismaleimide Resin (Specimen Cycled at 48.2 MPa, i.e., 7.0 ksi, Failed at 15,250 Cycles).

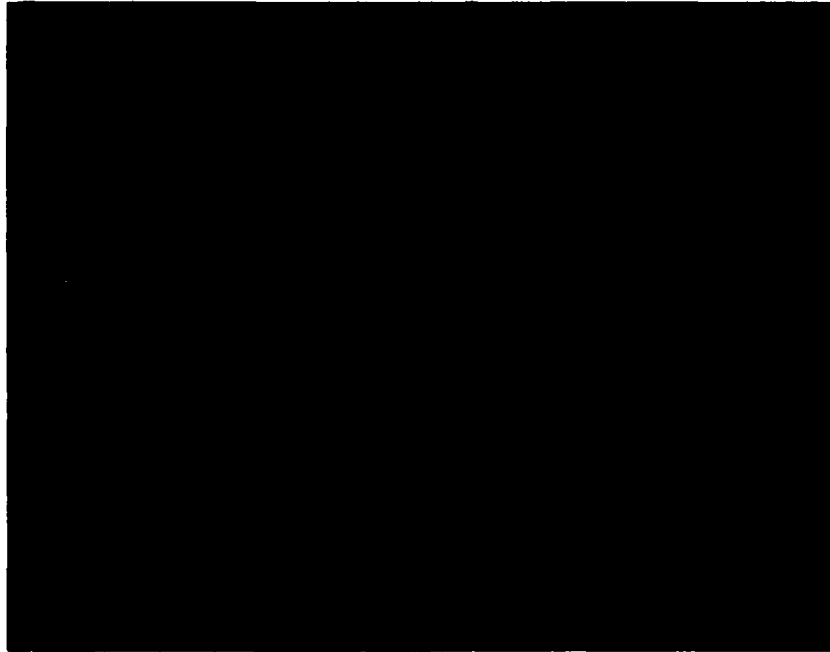


a) Overall View of Specimen Failure Surface



b) Close-up of Failure Initiation Site

Figure D21. Tension Fatigue, Specimen No. NTEX04, 88°C Test of Hercules X4001 Neat Bismaleimide Resin (Specimen Cycled at 35.1 MPa, i.e., 5.1 ksi, Failed at 528,440 Cycles).



a) Overall View of Specimen Failure Surface



b) Close-up of Failure Initiation Site

Figure D22. Tension Fatigue, Specimen No. NTEX07, 88°C Test of Hercules X4001 Neat Bismaleimide Resin (Specimen Cycled at 37.2 MPa, i.e., 5.4 ksi, Failed at 28,180 Cycles).



a) Overall View of Specimen Failure Surface



b) Close-up of Failure Initiation Site

Figure D23. Tension Fatigue, Specimen No. NTEX02, 88°C Test of Hercules X4001 Neat Bismaleimide Resin (Specimen Cycled at 41.3 MPa, i.e., 6.0 ksi, Failed at 1,806 Cycles).

NADC-83053-60

THIS PAGE INTENTIONALLY LEFT BLANK

APPENDIX E
MOISTURE DISTRIBUTION ANALYSIS PARAMETERS

NADC-83053-60

THIS PAGE INTENTIONALLY LEFT BLANK

APPENDIX E

MOISTURE DISTRIBUTION ANALYSIS PARAMETERS

The linear moisture distribution in a triangular axisymmetric element with i, j and k nodal circles is expressed as

$$M = N_i M_i + N_j M_j + N_k M_k \quad (E-1)$$

where N_i , N_j and N_k are the shape functions and M_i , M_j and M_k are the nodal moisture content values.

The shape functions in the r and z coordinate system are:

$$\begin{aligned} N_i &= [a_i + b_i r + c_i z] \\ N_j &= [a_j + b_j r + c_j z] \end{aligned} \quad (E-2)$$

$$\text{and } N_k = [a_k + b_k r + c_k z]$$

where A is the area of the triangular cross section of the element and

$$\begin{aligned} a_i &= r_j z_k - r_k z_j, & b_i &= z_j - z_k, & c_i &= r_k - r_j \\ a_j &= r_k z_i - r_i z_k, & b_j &= z_k - z_i, & c_j &= r_i - r_k \\ a_k &= r_i z_j - r_j z_i, & b_k &= z_i - z_j, & c_k &= r_j - r_i \end{aligned}$$

The Element Diffusivity Matrix is

$$\begin{aligned} [g]_e &= \frac{2\pi\bar{r}^2 D_{rr}}{4A} \begin{bmatrix} b_i b_i & b_i b_j & b_i b_k \\ b_i b_j & b_j b_j & b_j b_k \\ b_i b_k & b_j b_k & b_k b_k \end{bmatrix} \\ &+ \frac{2\pi\bar{r}^2 D_{zz}}{4A} \begin{bmatrix} c_i c_i & c_i c_j & c_i c_k \\ c_i c_j & c_j c_j & c_j c_k \\ c_i c_k & c_j c_k & c_k c_k \end{bmatrix} \end{aligned} \quad (E-3)$$

$$\text{where } \bar{r} = (r_i + r_j + r_k)/3.$$

The Element Capacitance Matrix is

$$[P]_e = B \begin{bmatrix} P_{11} & P_{12} & P_{13} \\ P_{12} & P_{22} & P_{23} \\ P_{13} & P_{23} & P_{33} \end{bmatrix} \quad (E-4)$$

where $B = 2\pi A/180$

$$\begin{aligned} P_{11} &= [12r_i^2 + 2r_j^2 + 2r_k^2 + 6r_i r_j + 6r_i r_k + 2r_j r_k] \\ P_{12} &= [3r_i^2 + 3r_j^2 + r_k + 4r_i r_j + 2r_i r_k + 2r_j r_k] \\ P_{13} &= [3r_i^2 + r_j^2 + 3r_k^2 + 2r_i r_j + 4r_i r_k + 2r_j r_k] \\ P_{22} &= [2r_i^2 + 12r_j^2 + 2r_k^2 + 6r_i r_j + 2r_i r_k + 6r_j r_k] \\ P_{23} &= [r_i^2 + 3r_j^2 + 3r_k^2 + 2r_i r_j + 2r_i r_k + 4r_j r_k] \\ P_{33} &= [2r_i^2 + 2r_j^2 + 12r_k^2 + 2r_i r_j + 6r_i r_k + 6r_j r_k] \end{aligned}$$

Non-Government Agencies (continued)

	<u>No. of Copies</u>
University of Wyoming, Laramie, WY 82071 (Attn: Dr. D. Adams).	1
Villanova University, Villanova, PA 19085 (Attn: Dr. P. V. McLaughlin)	1
Virginia Polytechnic Institute, Blacksburg, VA 24061 (Attn: Dr. K. Reifsnider)	1
Vought Corporation, Dallas, TX 75265 (Attn: Mr. O. E. Dhonau/2-53442)	1
(Attn: Dr. J. Renton)	1

Non-Government Agencies (continued)

	<u>No. of Copies</u>
McDonnell Douglas Corporation, St. Louis, MO 63166	
(Attn: Mr. J. Schier)	1
(Attn: Mr. C. Stenberg)	1
(Attn: Mr. R. Garrett)	1
McDonnell Douglas Corporation, Long Beach, CA 90846	
(Attn: G. Lehman)	1
(Attn: D. Smillie)	1
Minnesota Mining and Manufacturing Company, St. Paul, MN 55104	
(Attn: Mr. W. Davis)	1
Northrop Aircraft Corporation, One Northrop Avenue, Hawthorne, CA 90250 (Attn: Mr. L. Jeans)	1
(Attn: Mr. D. Stansbarger)	1
(Attn: Mr. R. C. Isemann)	1
(Attn: Mr. R. M. Verette)	1
(Attn: Mr. B. Butler)	1
Owens Corning Fiberglass, Granville, OH 43023	
(Attn: Mr. D. Mettes)	1
Prototype Development Associates, Inc., 1560 Brookhollow Drive, Santa Ana, CA 92705 (Attn: E. L. Stanton)	1
Rockwell International, Columbus, OH 43216	
(Attn: Mr. F. Kaufman)	1
(Attn: Mr. M. Schweiger)	1
Rockwell International, Los Angeles, CA 90009	
(Attn: Dr. Lackman)	1
Rockwell International, Tulsa, OK 74151	
(Attn: Mr. E. Sanders)	1
(Attn: Mr. J. H. Powell)	1
Rohr Corporation, Riverside, CA 92503	
(Attn: Dr. F. Riel)	1
(Attn: Mr. R. Elkin)	1
School of Engineering and Applied Science, Materials Research Laboratory, Washington University, Campus Box 1087, St. Louis, MO 63130 (Attn: T. Hahn)	1
Sikorsky Aircraft, Stratford, CT 06622	
(Attn: Mr. J. Ray)	1
Teledyne Ryan Aeronautical Company, San Diego, CA 92138	
(Attn: Mr. R. Long)	1
Union Carbide Corporation, Cleveland, OH 44101	
(Attn: Dr. H. F. Volk)	1
University of Dayton Research Institute, 300 College Park Ave., Dayton, OH 45469 (Attn: Dr. J. Gallagher)	1
University of Delaware, Mechanics & Aerospace Eng. Dept., Evans Hall, Newark, DE 19711 (Attn: Dr. R. B. Pipes)	1
University of Oklahoma, Norman, OK 73019	
(Attn: Dr. C. W. Bert, School of AMNE)	1

Non-Government Agencies (continued)

	<u>No. of Copies</u>
Effects Technology, Inc., 5383 Hollister Avenue, P. O. Box 30400, Santa Barbara, CA 93111 (Attn: Robert Globus) . .	1
E. I. DuPont Company, Wilmington, DE 19898 (Attn: Dr. J. Pigoiacampi)	1
Fairchild Republic Company, Farmingdale, L. I., NY 11735 (Attn: Mr. Frank Costa)	1
Georgia Institute of Technology, Atlanta, GA (Attn: Prof. W. H. Horton)	1
General Dynamics/Convair, San Diego, CA 92138 (Attn: Mr. D. R. Dunbar)	1
(Attn: Mr. W. G. Scheck)	1
General Dynamics, Fort Worth, TX 76101 (Attn: Mr. J. A. Fant)	1
(Attn: Dr. D. Wilkins (Composite Structures Eng. Dept.) . .	1
General Electric Company, Phila., PA 19101 (Attn: Dr. C. Zweben)	1
(Attn: Mr. A. Garber)	1
Great Lakes Carbon Corporation, NY, New York 10017 (Attn: Mr. W. R. Benn, Mgr., Market Development)	1
Grumman Aerospace Corporation, South Oyster Bay Rd., Bethpage, Long Island, NY 11714 (Attn: Mr. R. Hadcock)	1
(Attn: Mr. S. Dastin)	1
Hercules Aerospace Division, P. O. Box 210, Cumberland, MD 21502 (Attn: Mr. D. Hug)	1
HITCO, 1600 West 135th Street, Gardena, CA 90249 (Attn: Mr. N. Myers)	1
ITT Research Institute, Chicago, IL 60616 (Attn: Mr. K. Hofar)	1
J. P. Stevens & Co., Inc., New York, NY 10036 (Attn: Mr. H. I. Shulock)	1
Kaman Aircraft Corporation, Bloomfield, CT 06002 (Attn: Technical Library)	1
Lehigh University, Bethlehem, PA 18015 (Attn: Dr. G. C. Sih)	1
Lockheed-California Co., Burbank, CA 91520 (Attn: Mr. E. K. Walker)	1
(Attn: Mr. Vaughn)	1
(Attn: Mr. A. James)	1
Lockheed-California Co., Rye Canyon Research Lab, Burbank, CA 91520 (Attn: Mr. Don E. Pettit)	1
Lockheed-Georgia Company, Marietta, GA 30063 (Attn: Technical Information Dept., Dept. 72-34, Zone 26) .	1
Materials Sciences Corporation, Spring House, PA 19477	1
Philadelphia College of Textiles and Science, School House Lane and Henry Ave., Philadelphia, PA 19144 (Attn: Dr. Frank Ko)	1

Government Activities (continued)

	<u>No. of Copies</u>
NOL, White Oak, MD 20910 (Attn: Mr. F. R. Barnet)	1
NRL, Washington, D.C. 20375 (Attn: Dr. I. Wolock)	1
ONR, Washington, D.C. 20362 (Attn: Dr. N. Perrone)	1
PLASTEC, Picatinny Arsenal, Dover, NJ 07801 (Attn: Mr. H. Pebly)	1
(Attn: Librarian, Code DRDAR-SCM-0, Bldg. 351-N.	1
U. S. Army Materials and Mechanics Research Center (DRXMR-PL) Watertown, MA 02172 (Attn: Dr. E. Lenoe)	1
(Attn: Mr. D. Oplinger)	1
U. S. Army Research Office, Durham, NC 27701	1
U. S. Army R&T Lab (AVRADCOM), Ames Research Center, Moffett Field, CA 94035 (Attn: Mr. F. Immen, DAVDL-AS-M.S. 207-5, Dr. R. Foye)	2
David Taylor Naval Ship Research & Development Center, Code 2822, Annapolis, MD 21402 (Attn: Mr. A. Macander, Mr. R. Crane)	2

Non-Government Activities

Avco, Aero Structures Division, Nashville, TN 37210	1
Battelle Columbus Laboratories, Metals and Ceramics Information Center, 505 King Avenue, Columbus, OH 43201	1
Bell Aerospace Company, Buffalo, NY 14240 (Attn: Zone I-85, Mr. F. M. Anthony)	1
Bell Helicopter Company, Fort Worth, TX 76101 (Attn: Mr. G. Reis Alsmiller, Jr.)	1
Bendix Products Aerospace Division, South Bend, IN 46619 (Attn: Mr. R. V. Cervelli)	1
Boeing Company, P. O. Box 3707, Seattle, WA 98124 (Attn: Mr. R. E. Horton, MS 9K-23)	1
(Attn: Dr. R. June)	1
Boeing Company, Vertol Division, P. O. Box 16858, Philadelphia, PA 19142 (Attn: Mr. R. L. Pinckney)	1
(Attn: Mr. D. Hoffstedt)	1
(Attn: Mr. L. Marchinski)	1
Boeing Company, Wichita, KS 67210 (Attn: R. D. Hoaglanb - M. S. -K32-95)	1
Cabot Corporation, Billerica Research Center, Billerica, MA 01821	1
Composittek Engineering Corporation, 6925-1 Aragon Circle, Buena Park, CA 90620 (Attn: J. V. Noyes)	1
Drexel University, Phila., PA 19104 (Attn: Dr. P. C. Chou)	1
(Attn: Dr. A. S. D. Wang)	1

END

FILMED

1-84

DTIC